Model reduction based on matrix interpolation and distorted finite element meshes for dynamic analysis of 2D nearly periodic structures

Jean-Mathieu Mencik

Version of Record: https://www.sciencedirect.com/science/article/pii/S0168874X21000020
Manuscript_06669edc2218ba4504a3d3bd96e45724

Model reduction based on matrix interpolation and distorted finite element meshes for dynamic analysis of 2D nearly periodic structures

Jean-Mathieu Mencik

INSA Centre Val de Loire, Université d'Orléans, Université de Tours, Laboratoire de Mécanique Gabriel Lamé, Rue de la Chocolaterie, 41000 Blois, France

Abstract

The dynamic analysis of 2D nearly periodic structures of finite dimensions, subject to harmonic excitations, is addressed. Such structures are often made up of slightly different locally resonant layered substructures whose geometrical properties randomly vary in space and which are described here by means of distorted finite element (FE) meshes. It is well known that purely periodic structures with resonant substructures possess band gap properties, i.e., frequency bands where the vibration levels are low. The question arises whether nearly periodic structures provide additional features, e.g., the fact that the vibrational energy remains localized around the excitation points. Predicting the harmonic responses of such structures via efficient numerical approaches is the motivation behind the present paper. Usually, the Craig Bampton (CB) method is used to model the substructures in terms of reduced mass and stiffness matrices, which can be further assembled together to model a whole structure. The issue arises because the reduced mass and stiffness matrices of the substructures need to be computed several times — i.e., for several substructures whose properties differ to each other —, which is computationally cumbersome. To address this issue, a strategy is proposed which involves computing the reduced matrices of the substructures for some particular distorted FE meshes (a few number), and interpolating these matrices between these "interpolation points" for modeling substructures with random FE meshes. The relevance of the interpolation strategy, in terms of computational time saving and accuracy, is highlighted through comparisons with the FE and CB methods. Three structures are analyzed, i.e., (1) a plate with 8×8 substructures, (2) a plate with 15×15 substructures, and (3) a plate with 8×4 substructures embedded in a floor panel. Results show that, at high frequencies, the vibration levels of the nearly periodic structures undergo an overall reduction compared to the purely periodic cases.

Key words: nearly periodic structures, finite elements, dynamic substructuring, matrix interpolation.

1. Introduction

This paper aims at analyzing the dynamic behavior of 2D nearly periodic structures, of finite dimensions, subject to harmonic excitations. Such structures can be made up, for instance, of slightly different locally resonant substructures whose geometrical properties randomly vary in space. This topic is mostly linked to that of resonant metamaterials which has gained a growing interest over the past years. For instance, a schematic of a 2D nearly periodic plate with 5×5 substructures embedded in a floor panel is shown in Fig. 1 along with the transverse displacement field of the whole structure (plate and panel, at a certain frequency). In this case, the substructures are multi-layered, i.e., composed of a medium layer with soft material (green part) and a heavy core (black part) — i.e., which behave like a single or multi-DOF mass-spring system — whose dimensions are subject to small variabilities. This yields substructures with different resonance frequencies, and therefore, nearly periodic structures which can behave in a completely different way than purely periodic structures. The key idea behind the present work is that the substructure variabilities are introduced by means of distorted

Email address: jean-mathieu.mencik@insa-cvl.fr (Jean-Mathieu Mencik)

FE meshes with node coordinates defined by means of deterministic space functions weighted by random variables, e.g., trigonometric functions as shown in Fig. 1. This involves moving the nodes of a baseline mesh (purely periodic case) to obtain substructures with different node coordinates, and therefore, different parametrization and geometrical properties. Also, since the substructures are modeled using different random variables, they do not share the same distorted mesh and geometrical properties. For periodic structures with identical substructures, it is well known that locally resonant band gaps occur — i.e., frequency bands with low displacement levels — which appear to be interesting in passive vibration control of structures. The question which is addressed here is whether the use of nearly periodic structures provides additional features, e.g., the fact that the vibrational energy is localized around the excitation points (as already reported in the literature [1, 2]).

This paper does not aim at providing a comprehensive analysis neither about the band gap effect in periodic structures nor the band gap and localization effects in nearly periodic structures. There already exist numerous works on these topics, see for instance [3–7] for band-structure calculations in periodic structures, [1, 2, 8] for localization effects in 1D nearly periodic structures and 1D disordered phononic crystals, and [9] for localization effects in 1D banded structures. Instead, the present paper aims at proposing reduced models of 2D nearly periodic structures (also applicable to purely periodic structures), of finite dimensions, which can be quickly solved to predict their harmonic response. The problem which is tackled here is that of structures made up of several substructures which need to be discretized with a sufficient number of nodes and degrees of freedom (DOFs) to meet accurate results over the frequency bands analyzed, which as such yield large-sized FE models. The proposed approach is intended to be general and could be applied, in theory, to any kind of structures which are 2D periodic. However, for the sake of simplicity and in order to target the specific but interesting topic of 2D metamaterials which is broadly explored nowadays, plane structures made up of "resonant" layered substructures will be only considered (see Fig. 1).

For purely periodic structures, there exist well-suited model reduction strategies based on component modes and reduced (mass and stiffness) matrices of the substructures. Especially, the Craig Bampton (CB) method [10, 11] constitutes an efficient means to obtain these reduced matrices. Within this framework, a projection vector subspace is used which is spanned by the static modes and a reduced number of fixed interface modes of the substructures. Since the substructures are identical, they share the same component modes — i.e., the same static modes and fixed interface modes — and, therefore, the same reduced mass and stiffness matrices. In other words, the component modes and the reduced matrices of the substructures only need to be computed once, regardless of the number of substructures considered. The modeling of a whole periodic structure follows from FE assembly procedures, i.e., by assembling the reduced matrices of the substructures together to build the global mass and stiffness matrices of the periodic structure. There exist other well-suited approaches, e.g., those based on Bloch waves which are good numerical means to predict the dynamic response of 2D periodic structures which are infinite, or which are assumed to be infinite (i.e., damped with large dimensions), subject to point forces [12, 13]. However, all these approaches invoke the periodic nature of the structures and are therefore not suitable to handle nearly periodic structures, i.e., when the substructures are different to each other. In this case, the component modes and the reduced matrices have to be computed as many times as the number of substructures considered. The issue is that the computational load involved in the repetition of these numerical tasks linearly grows as a function of the number of substructures considered, and can rapidly surpass that involved in the assembly of the substructures, even that required by the classic FE method for modeling a whole structure.

Several approaches can be used to circumvent the computational burden associated with the repetition of the numerical tasks mentioned earlier. Among these approaches, one can mention the subspace enrichment techniques that would consist in computing the component modes of the substructures for one or several particular distorted meshes, and using these component modes together with additional Ritz vectors for modeling substructures with random FE meshes. The readers are referred to [14–17] for a general overview of these techniques. A second class of approaches, which is investigated in this paper, involves interpolating the reduced matrices of the substructures between some "interpolation points" which in the present case concern some par-

ticular distorted meshes. The readers are referred to [18–21]. The key idea is to consider a few interpolation points which are similar for each substructure analyzed. The computational load involved in the computation of the reduced matrices at these few points is not high. The remaining task involves interpolating the matrices between these points via appropriate interpolation functions, which is low-time consuming.

Interpolating the reduced mass and stiffness matrices requires a special care, however, in the sense that two matrices computed for two particular distorted meshes can strongly differ to each other, even though the mesh distortion is small. In [18–21], a congruence transformation is used in order to describe the reduced matrices in coordinate systems which are compatible to each other. This can be understood as reordering and scaling the column vectors of the reduced matrices of fixed interface modes of the substructures, computed for different distorted meshes, in order to make them close to each other. Following the idea in [18], a strategy can be proposed which involves considering a "common matrix" whose column range is close to those of the matrices of fixed interface modes, and projecting this common matrix onto the matrices of fixed interface modes to define "new" reduced matrices. In the present work, the common matrix is not exactly similar to that proposed in [18] and is expressed by means of the matrix of fixed interface modes of the substructures without distorted meshes (periodic case). The determination of the interpolated reduced matrices follows by considering an interpolation scheme based on eight interpolation points and eight Serendipity interpolation functions.

The modeling of an assembly involving several substructures is carried out via FE assembly procedures. For computational purposes, a second model reduction is considered which consists in expressing the displacement vector of the substructure boundary nodes using the vibration modes of the equivalent periodic structure (without distorted meshes).

The rest of the paper is organized as follows. The FE and CB modelings of plane structures which are 2D periodic and 2D nearly periodic are presented in Sec. 2. The issues involved in the modeling of nearly periodic structures are discussed. The interpolation strategy for modeling the reduced mass and stiffness matrices of the substructures is detailed in Sec. 3. Also, the strategy to model a whole 2D nearly periodic structure, and an assembly involving several nearly periodic and (purely) periodic structures, is presented. Numerical results are finally proposed in Sec. 4. Three test cases are considered, i.e., (1) a plate with 8×8 substructures, (2) a plate with 15×15 substructures, and (3) a plate with 8×4 substructures embedded in a floor panel. The relevance of the interpolation strategy, in terms of computational time saving and accuracy, is discussed through comparisons with the FE and CB methods.

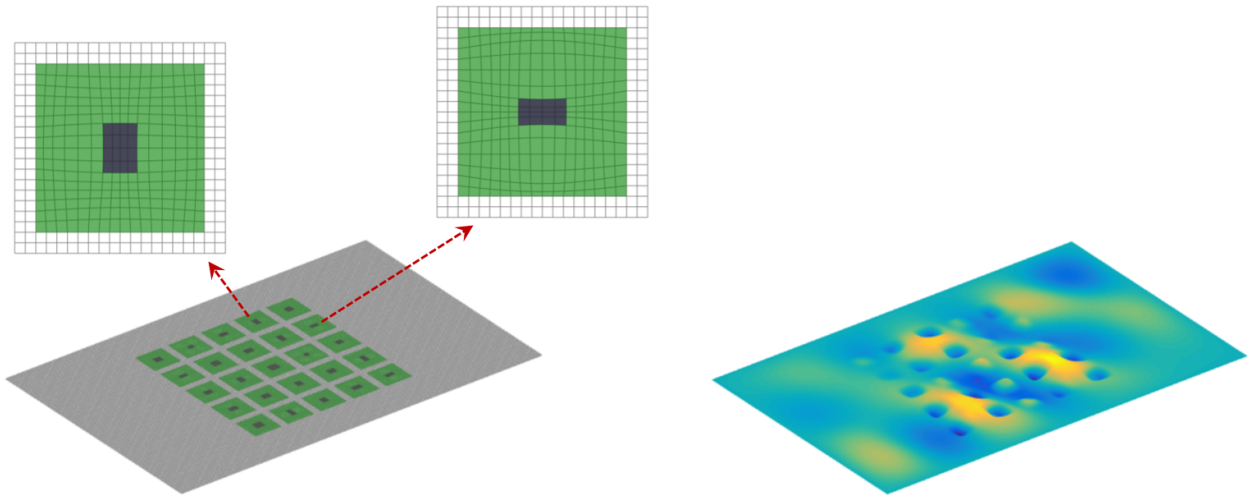

Figure 1: Schematic of a nearly periodic plate (distorted meshes of the substructures) embedded in a floor panel, and related transverse displacement field resulting from harmonic excitations.

2. Problem description

This first part aims at presenting the strategy for modeling plane structures, which are 2D periodic or 2D nearly periodic, using the FE method and the related CB substructuring technique. Especially, the issues raised by the modeling of nearly periodic structures are emphasized.

Let us start with a periodic structure which can be of rectangular shape as shown in Fig. 2, consisting of a finite number of identical square substructures with the same FE meshes which are assembled together along two perpendicular $x-$ and $y-$directions. These substructures are supposed to be linear, elastic, dissipative and isotropic, with material properties which vary in space ($x-$ and $y-$directions). For instance, a substructure made up of three layers having different material properties is shown in Fig. 2. Since the substructures are identical and are modeled with the same FE mesh, they share the same mass, damping and stiffness matrices $\mathbf{M}$, $\mathbf{C}$ and $\mathbf{K}$. In this sense, the dynamic equilibrium equation of a certain substructure s can be expressed in the frequency domain as follows:

$$\left[-\omega^2\mathbf{M} + \mathtt{i}\omega\mathbf{C} + \mathbf{K}\right]\mathbf{u}^s = \mathbf{F}^s, \tag{1}$$

where $\mathbf{u}^s$ and $\mathbf{F}^s$ are vectors of displacements and forces (respectively), ω is the angular frequency and $\mathtt{i}$ is the imaginary unit. For the sake of simplicity, assumption is made that the damping matrix $\mathbf{C}$ is of Rayleigh type, i.e., it is proportional to the mass and stiffness matrices:

$$\mathbf{C} = a\mathbf{M} + b\mathbf{K}, \tag{2}$$

where a and b are two positive real constants. Thus, Eq. (1) can be rewritten as follows:

$$\left[(-\omega^2 + \mathtt{i}\omega a)\mathbf{M} + (\mathtt{i}\omega b + 1)\mathbf{K}\right]\mathbf{u}^s = \mathbf{F}^s. \tag{3}$$

Assume that the substructures are meshed using isoparametric elements with interpolation functions $N_j^e(\xi,\eta)$ where ξ and η are parametric coordinates. For each element e, the Jacobian matrix — which expresses the derivatives of the physical coordinates (x, y) with respect to the parametric coordinates (ξ, η) — is given by [22]:

$$\mathbf{J}^e(\xi,\eta) = \begin{bmatrix} \frac{\partial x}{\partial \xi} & \frac{\partial x}{\partial \eta} \\ \frac{\partial y}{\partial \xi} & \frac{\partial y}{\partial \eta} \end{bmatrix} = \begin{bmatrix} \sum_{j=1}^{n^e} \frac{\partial N_j^e(\xi,\eta)}{\partial \xi} x_j^e & \sum_{j=1}^{n^e} \frac{\partial N_j^e(\xi,\eta)}{\partial \eta} x_j^e \\ \sum_{j=1}^{n^e} \frac{\partial N_j^e(\xi,\eta)}{\partial \xi} y_j^e & \sum_{j=1}^{n^e} \frac{\partial N_j^e(\xi,\eta)}{\partial \eta} y_j^e \end{bmatrix}, \tag{4}$$

where n^e is the number of nodes of the element, and (x_j^e, y_j^e) are the node coordinates. Let us assume that each element has uniform material properties and constant height h^e. In this sense, the mass and stiffness matrices of an element e — namely, $\mathbf{M}^e$ and $\mathbf{K}^e$ — can be expressed as follows [22, 23]:

$$\mathbf{M}^e = \rho^e h^e \int_{\Omega_{\boldsymbol{\xi}}^e} \mathbf{N}^e(\xi,\eta)^T \mathbf{N}^e(\xi,\eta)\, J^e(\xi,\eta)\, d\xi d\eta \quad , \quad \mathbf{K}^e = h^e \int_{\Omega_{\boldsymbol{\xi}}^e} \mathbf{B}^e(\xi,\eta)^T \mathbf{H}^e \mathbf{B}^e(\xi,\eta)\, J^e(\xi,\eta)\, d\xi d\eta, \tag{5}$$

where $\Omega_{\boldsymbol{\xi}}^e$ is the 2D "parametric" domain occupied by the element, ρ^e is the density, $\mathbf{N}^e(\xi,\eta)$ is the matrix of interpolation functions $N_j^e(\xi,\eta)$, $\mathbf{H}^e$ is the matrix of elastic constants, and $J^e(\xi,\eta) = \mathtt{det}[\mathbf{J}^e(\xi,\eta)]$. Also, $\mathbf{B}^e(\xi,\eta)$ is a matrix whose expression depends on the type of element considered. It is expressed from the derivatives of the interpolation functions $N_j^e(\xi,\eta)$ with respect to x and y, which are obtained as follows:

$$\begin{bmatrix} \frac{\partial N_j^e(\xi,\eta)}{\partial x} \\ \frac{\partial N_j^e(\xi,\eta)}{\partial y} \end{bmatrix} = \mathbf{J}^e(\xi,\eta)^{-T} \begin{bmatrix} \frac{\partial N_j^e(\xi,\eta)}{\partial \xi} \\ \frac{\partial N_j^e(\xi,\eta)}{\partial \eta} \end{bmatrix}, \tag{6}$$

where superscript $-T$ denotes the inverse of the transpose (superscript T). Notice that the matrices $\mathbf{M}^e$ and $\mathbf{K}^e$ are of size $N^e \times N^e$ where N^e is the number of degrees of freedom (DOFs) of the element, i.e., $N^e = n^e d$ where d is the number of DOFs per node. Following the FE procedure, the mass and stiffness matrices of the substructures are built by assembling the mass and stiffness matrices of the elements as follows:

$$\mathbf{M} = \sum_e (\mathbf{L}^e)^T \mathbf{M}^e \mathbf{L}^e \quad , \quad \mathbf{K} = \sum_e (\mathbf{L}^e)^T \mathbf{K}^e \mathbf{L}^e, \tag{7}$$

where $\mathbf{L}^e$ are the (Boolean) localization matrices of the elements. The mass and stiffness matrices of a whole 2D periodic structure (Fig. 2) are finally obtained by assembling the mass and stiffness matrices of the substructures, in the same way as Eq. (7). This yields:

$$\mathbf{M}_{\mathtt{per}} = \sum_s (\mathbf{L}^s)^T \mathbf{M} \mathbf{L}^s \quad , \quad \mathbf{K}_{\mathtt{per}} = \sum_s (\mathbf{L}^s)^T \mathbf{K} \mathbf{L}^s, \tag{8}$$

where $\mathbf{L}^s$ are the localization matrices of the substructures.

It is worth pointing out that, from the numerical point of view, the space integrals involved in Eq. (5) are usually computed via Gauss point quadrature, while the matrix assemblies in Eqs. (7) and (8) are performed via DOF connectivity vectors.

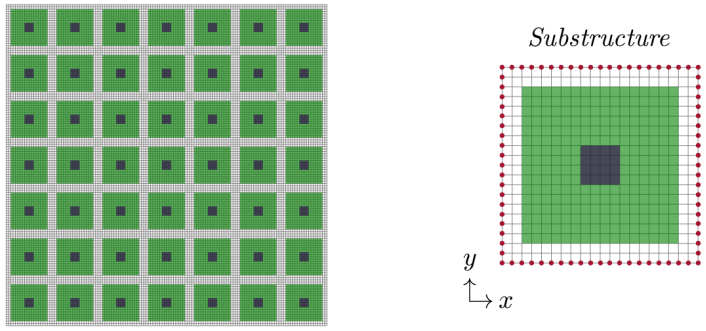

Figure 2: 2D periodic structure and FE mesh of a substructure (red spots highlight boundary nodes).

For computational purposes, reduced matrices $\widetilde{\mathbf{M}}$ and $\widetilde{\mathbf{K}}$ of the substructures are usually considered to reduce the size of the global FE model. Especially, the CB substructuring technique provides an efficient means to perform model reduction. The key steps of the CB method can be summarized as follows [11]. Let us write the mass and stiffness matrices $\mathbf{M}$ and $\mathbf{K}$ of the substructures, as well as the displacement and force vectors $\mathbf{u}^s$ and $\mathbf{F}^s$, as follows:

$$\mathbf{M} = \begin{bmatrix} \mathbf{M}_{\mathtt{BB}} & \mathbf{M}_{\mathtt{BI}} \\ \mathbf{M}_{\mathtt{IB}} & \mathbf{M}_{\mathtt{II}} \end{bmatrix} \quad , \quad \mathbf{K} = \begin{bmatrix} \mathbf{K}_{\mathtt{BB}} & \mathbf{K}_{\mathtt{BI}} \\ \mathbf{K}_{\mathtt{IB}} & \mathbf{K}_{\mathtt{II}} \end{bmatrix} \quad , \quad \mathbf{u}^s = \begin{bmatrix} \mathbf{u}^s_{\mathtt{B}} \\ \mathbf{u}^s_{\mathtt{I}} \end{bmatrix} \quad , \quad \mathbf{F}^s = \begin{bmatrix} \mathbf{F}^s_{\mathtt{B}} \\ \mathbf{F}^s_{\mathtt{I}} \end{bmatrix}, \tag{9}$$

where subscript $\mathtt{B}$ refers to the boundary DOFs (see red spots highlighted in Fig. 2), and subscript $\mathtt{I}$ refers to the internal DOFs (i.e., those which do not belong to the boundary). Note that the mass and stiffness matrices $\mathbf{M}$ and $\mathbf{K}$ are symmetric, which means that $\mathbf{M}^T_{\mathtt{BB}} = \mathbf{M}_{\mathtt{BB}}$, $\mathbf{K}^T_{\mathtt{BB}} = \mathbf{K}_{\mathtt{BB}}$, $\mathbf{M}^T_{\mathtt{II}} = \mathbf{M}_{\mathtt{II}}$, $\mathbf{K}^T_{\mathtt{II}} = \mathbf{K}_{\mathtt{II}}$, $\mathbf{M}^T_{\mathtt{IB}} = \mathbf{M}_{\mathtt{BI}}$ and $\mathbf{K}^T_{\mathtt{IB}} = \mathbf{K}_{\mathtt{BI}}$.

Introduce the matrix of fixed interface modes $\mathbf{X} = [\boldsymbol{\chi}_1 \boldsymbol{\chi}_2 \cdots \boldsymbol{\chi}_{N_{\mathtt{I}}}]$ where $N_{\mathtt{I}}$ is the number of internal DOFs of the substructures, and where $\boldsymbol{\chi}_k$ ($k = 1, \ldots, N_{\mathtt{I}}$) refers to the eigenvectors of the matrix pencil $(\mathbf{K}_{\mathtt{II}}, \mathbf{M}_{\mathtt{II}})$. Those modes are usually normalized with respect to the mass matrix $\mathbf{M}_{\mathtt{II}}$, i.e.:

$$\boldsymbol{\chi}_k \rightarrow \frac{\boldsymbol{\chi}_k}{\left(\boldsymbol{\chi}_k^T \mathbf{M}_{\mathtt{II}} \boldsymbol{\chi}_k\right)^{\frac{1}{2}}}. \tag{10}$$

In this way, it can be shown that the modes are orthogonal with respect to the mass matrix $\mathbf{M}_{\mathtt{II}}$, i.e., $\boldsymbol{\chi}_k^T \mathbf{M}_{\mathtt{II}} \boldsymbol{\chi}_l = \delta_{kl}$ (δ_{kl} being the Kronecker delta). Then, extract a reduced matrix of fixed interface modes from $\mathbf{X}$, i.e., $\widetilde{\mathbf{X}} = [\boldsymbol{\chi}_1 \boldsymbol{\chi}_2 \cdots \boldsymbol{\chi}_{M_{\mathtt{I}}}]$ where $M_{\mathtt{I}} < N_{\mathtt{I}}$, and approximate the displacement vector $\mathbf{u}_{\mathtt{I}}^s$ as follows:

$$\mathbf{u}_{\mathtt{I}}^s \approx \widetilde{\mathbf{u}}_{\mathtt{I}}^s = -(\mathbf{K}_{\mathtt{II}})^{-1} \mathbf{K}_{\mathtt{IB}} \widetilde{\mathbf{u}}_{\mathtt{B}}^s + \widetilde{\mathbf{X}} \widetilde{\boldsymbol{\alpha}}^s, \tag{11}$$

where $-(\mathbf{K}_{\mathtt{II}})^{-1}\mathbf{K}_{\mathtt{IB}}$ is the so-called matrix of static modes — i.e., those issued by considering the static response of a substructure when unit displacements are successively applied to the boundary DOFs, the other being clamped —, and $\widetilde{\boldsymbol{\alpha}} = [\widetilde{\alpha}_1 \widetilde{\alpha}_2 \cdots \widetilde{\alpha}_{M_{\mathtt{I}}}]^T$ is the so-called vector of generalized coordinates. Notice that the size of the matrix $-(\mathbf{K}_{\mathtt{II}})^{-1}\mathbf{K}_{\mathtt{IB}}$ is $N_{\mathtt{I}} \times N_{\mathtt{B}}$ where $N_{\mathtt{B}}$ is the number of boundary DOFs of the substructures. Also, in Eq. (11), $\widetilde{\mathbf{u}}_{\mathtt{I}}^s$ and $\widetilde{\mathbf{u}}_{\mathtt{B}}^s$ are approximates of $\mathbf{u}_{\mathtt{I}}^s$ and $\mathbf{u}_{\mathtt{B}}^s$, i.e., the displacement vectors computed when considering the reduced matrix $\widetilde{\mathbf{X}}$ instead of the full one $\mathbf{X}$. Then, introduce the transformation matrix $\widetilde{\mathbf{T}}$, defined such that:

$$\mathbf{u}^s \approx \widetilde{\mathbf{u}}^s = \begin{bmatrix} \widetilde{\mathbf{u}}_{\mathtt{B}}^s \\ \widetilde{\mathbf{u}}_{\mathtt{I}}^s \end{bmatrix} = \widetilde{\mathbf{T}} \begin{bmatrix} \widetilde{\mathbf{u}}_{\mathtt{B}}^s \\ \widetilde{\boldsymbol{\alpha}}^s \end{bmatrix}, \tag{12}$$

where

$$\widetilde{\mathbf{T}} = \begin{bmatrix} \mathbf{I}_{N_{\mathtt{B}}} & \mathbf{0} \\ -(\mathbf{K}_{\mathtt{II}})^{-1}\mathbf{K}_{\mathtt{IB}} & \widetilde{\mathbf{X}} \end{bmatrix}. \tag{13}$$

Invoking Eqs. (12) and (13) in Eq. (3), and left-multiplying the resulting equation by $\widetilde{\mathbf{T}}^T$, yields:

$$\left[(-\omega^2 + \mathtt{i}\omega a)\widetilde{\mathbf{M}} + (\mathtt{i}\omega b + 1)\widetilde{\mathbf{K}}\right] \begin{bmatrix} \widetilde{\mathbf{u}}_{\mathtt{B}}^s \\ \widetilde{\boldsymbol{\alpha}}^s \end{bmatrix} = \begin{bmatrix} \mathbf{F}_{\mathtt{B}}^s - \mathbf{K}_{\mathtt{BI}}(\mathbf{K}_{\mathtt{II}})^{-1}\mathbf{F}_{\mathtt{I}}^s \\ \widetilde{\mathbf{X}}^T \mathbf{F}_{\mathtt{I}}^s \end{bmatrix}, \tag{14}$$

where

$$\widetilde{\mathbf{M}} = \widetilde{\mathbf{T}}^T \mathbf{M} \widetilde{\mathbf{T}} \quad , \quad \widetilde{\mathbf{K}} = \widetilde{\mathbf{T}}^T \mathbf{K} \widetilde{\mathbf{T}}. \tag{15}$$

Eq. (14) is the dynamic equilibrium equation of the substructures expressed in the subspace spanned by the static modes and the reduced set of fixed interface modes. Within this framework, reduced mass and stiffness matrices $\widetilde{\mathbf{M}}$ and $\widetilde{\mathbf{K}}$ are considered whose size is $M \times M$ with $M < N$ (where $M = N_{\mathtt{B}} + M_{\mathtt{I}}$ and $N = N_{\mathtt{B}} + N_{\mathtt{I}}$). The reduced global mass and stiffness matrices of a whole 2D periodic structure follow from assembly procedures, by considering the displacement continuity conditions at the boundary DOFs. This yields:

$$\widetilde{\mathbf{M}}_{\mathtt{per}} = \sum_s (\widetilde{\mathbf{L}}^s)^T \widetilde{\mathbf{M}} \widetilde{\mathbf{L}}^s \quad , \quad \widetilde{\mathbf{K}}_{\mathtt{per}} = \sum_s (\widetilde{\mathbf{L}}^s)^T \widetilde{\mathbf{K}} \widetilde{\mathbf{L}}^s. \tag{16}$$

The global dynamic equilibrium equation of the periodic structure follows as:

$$\left[(-\omega^2 + \mathtt{i}\omega a)\widetilde{\mathbf{M}}_{\mathtt{per}} + (\mathtt{i}\omega b + 1)\widetilde{\mathbf{K}}_{\mathtt{per}}\right] \begin{bmatrix} (\widetilde{\mathbf{u}}_{\mathtt{B}})_{\mathtt{per}} \\ \widetilde{\boldsymbol{\alpha}}_{\mathtt{per}} \end{bmatrix} = \widetilde{\mathbf{F}}_{\mathtt{per}}, \tag{17}$$

where $(\widetilde{\mathbf{u}}_{\mathtt{B}})_{\mathtt{per}}$ is the displacement vector of the boundary/interface nodes of the substructures, and where:

$$\widetilde{\boldsymbol{\alpha}}_{\mathtt{per}} = \begin{bmatrix} \widetilde{\boldsymbol{\alpha}}^1 \\ \widetilde{\boldsymbol{\alpha}}^2 \\ \vdots \end{bmatrix} \quad , \quad \widetilde{\mathbf{F}}_{\mathtt{per}} = \sum_s (\widetilde{\mathbf{L}}^s)^T \begin{bmatrix} \mathbf{F}_{\mathtt{B}}^s - \mathbf{K}_{\mathtt{BI}}(\mathbf{K}_{\mathtt{II}})^{-1}\mathbf{F}_{\mathtt{I}}^s \\ \widetilde{\mathbf{X}}^T \mathbf{F}_{\mathtt{I}}^s \end{bmatrix}. \tag{18}$$

Concerning the boundary conditions (BCs) of the periodic structure, they may be written in a general way as follows:

$$\mathbf{Y}_{\mathtt{B}}(\widetilde{\mathbf{u}}_{\mathtt{B}})_{\mathtt{per}} + \mathbf{Z}_{\mathtt{B}}(\widetilde{\mathbf{F}}_{\mathtt{B}})_{\mathtt{per}} = \mathbf{Y}^0_{\mathtt{B}}(\widetilde{\mathbf{u}}_{\mathtt{B}})^0_{\mathtt{per}} + \mathbf{Z}^0_{\mathtt{B}}(\widetilde{\mathbf{F}}_{\mathtt{B}})^0_{\mathtt{per}}, \tag{19}$$

where $(\widetilde{\mathbf{u}}_{\mathtt{B}})^0_{\mathtt{per}}$ and $(\widetilde{\mathbf{F}}_{\mathtt{B}})^0_{\mathtt{per}}$ are vectors of prescribed displacements and prescribed forces, respectively, and where $\mathbf{Y}_{\mathtt{B}}$, $\mathbf{Z}_{\mathtt{B}}$, $\mathbf{Y}^0_{\mathtt{B}}$ and $\mathbf{Z}^0_{\mathtt{B}}$ are matrices whose expressions depend on the kind of applications considered. Here, $(\widetilde{\mathbf{F}}_{\mathtt{B}})_{\mathtt{per}}$ is the force vector for the boundary/interface nodes of the substructures, defined by:

$$(\widetilde{\mathbf{F}}_{\mathtt{B}})_{\mathtt{per}} = \sum_s (\widetilde{\mathbf{L}}^s)^T \mathbf{F}^s_{\mathtt{B}}. \tag{20}$$

Solving the matrix equation (17) with the BCs (19) yields the displacement vector $(\widetilde{\mathbf{u}}_{\mathtt{B}})_{\mathtt{per}}$ and the vector of generalized coordinates $\widetilde{\boldsymbol{\alpha}}_{\mathtt{per}}$. The displacement vector of the boundary nodes of a particular substructure s can be retrieved via a localization matrix $\widetilde{\mathbf{L}}^s_{\mathtt{B}}$, i.e., $\widetilde{\mathbf{u}}^s_{\mathtt{B}} = \widetilde{\mathbf{L}}^s_{\mathtt{B}}(\widetilde{\mathbf{u}}_{\mathtt{B}})_{\mathtt{per}}$. Also, the displacement vector $\widetilde{\mathbf{u}}^s = [(\widetilde{\mathbf{u}}^s_{\mathtt{B}})^T(\widetilde{\mathbf{u}}^s_{\mathtt{I}})^T]^T$ of this substructure can be retrieved by considering Eq. (12).

The CB method is advantageous in the sense it provides mass and stiffness matrices $\widetilde{\mathbf{M}}_{\mathtt{per}}$ and $\widetilde{\mathbf{K}}_{\mathtt{per}}$ of reduced size compared to the original matrices $\mathbf{M}_{\mathtt{per}}$ and $\mathbf{K}_{\mathtt{per}}$. This is explained because the mass and stiffness matrices of the substructures have a reduced size (as explained earlier). Hence, Eq. (17) can be quickly solved numerically. The key advantage is that, for purely periodic structures, the substructures share the same reduced matrices $\widetilde{\mathbf{M}}$ and $\widetilde{\mathbf{K}}$, which particularly means that the matrices of static modes $-(\mathbf{K}_{\mathtt{II}})^{-1}\mathbf{K}_{\mathtt{IB}}$ and fixed interface modes $\widetilde{\mathbf{X}}$ only need to be computed once. Things are more complicated when it comes to nearly periodic structures, i.e., when the substructures are not identical to each other. A nearly periodic structure involving slightly perturbed substructures with distorted FE meshes is shown in Fig. 3. For each substructure s, the distorted mesh is obtained by moving the positions of the nodes along the $x-$ and $y-$ directions as follows:

$$x^{se}_j = x^e_j + \epsilon^s_x f_x(x^e_j, y^e_j) \quad , \quad y^{se}_j = y^e_j + \epsilon^s_y f_y(x^e_j, y^e_j), \tag{21}$$

where (x^{se}_j, y^{se}_j) and (x^e_j, y^e_j) are the node coordinates of the distorted and undistorted meshes, respectively; ϵ^s_x and ϵ^s_y are uniform random variables with support $[-\delta\,,\,\delta]$ where δ is a dispersion parameter; $f_x(x,y)$ and $f_y(x,y)$ are two arbitrary deterministic functions of (x,y), identical for all the substructures, which are supposed to cancel out on the boundary. In this way, the coupling conditions between the substructures can be guaranteed. For instance, about the substructure displayed in Fig. 3, the functions $f_x(x,y)$ and $f_y(x,y)$ are chosen so that they are equal to zero over the first layer (light gray color), and vary sinusoidally elsewhere.

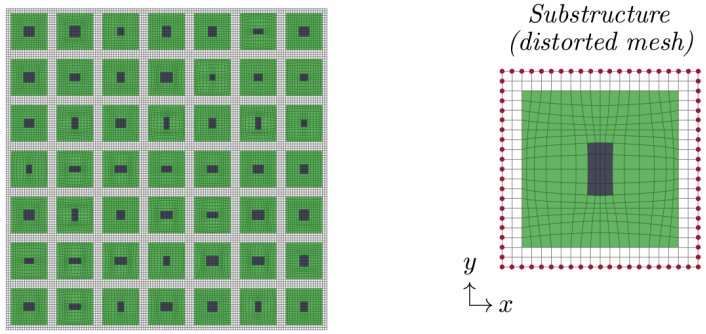

Figure 3: 2D nearly periodic structure and distorted FE mesh of a substructure (red spots highlight boundary nodes).

To sum up, the mass and stiffness matrices of the substructures — namely, $\mathbf{M}^s$ and $\mathbf{K}^s$ — are no more constant, as well as the reduced matrices $\widetilde{\mathbf{M}}^s$ and $\widetilde{\mathbf{K}}^s$. This is explained, first, because the Jacobian matrices of the elements are different between the substructures, i.e.,

$$\mathbf{J}^{se}(\xi,\eta) = \begin{bmatrix} \sum_{j=1}^{n^e} \frac{\partial N_j^e(\xi,\eta)}{\partial \xi} x_j^{se} & \sum_{j=1}^{n^e} \frac{\partial N_j^e(\xi,\eta)}{\partial \eta} x_j^{se} \\ \sum_{j=1}^{n^e} \frac{\partial N_j^e(\xi,\eta)}{\partial \xi} y_j^{se} & \sum_{j=1}^{n^e} \frac{\partial N_j^e(\xi,\eta)}{\partial \eta} y_j^{se} \end{bmatrix}. \tag{22}$$

In this case, the Jacobian matrices $\mathbf{J}^{se}(\xi,\eta)$ need to be expressed independently (for each substructure considered), which also means that the mass and stiffness matrices of the elements — namely, $\mathbf{M}^{se}$ and $\mathbf{K}^{se}$, see Eq. (5) — are not constant between the substructures, and therefore, that they have to be assembled (see Eq. (7)) as many times as the number of substructures involved. As a second shortcoming, the fact that the mass and stiffness matrices of the substructures $\mathbf{M}^s$ and $\mathbf{K}^s$ are not identical means that the matrices of static modes and fixed interface modes of the substructures — namely, $-(\mathbf{K}^s_{\mathtt{II}})^{-1}\mathbf{K}^s_{\mathtt{IB}}$ and $\widetilde{\mathbf{X}}^s$ — are not constant too. Hence, they need to be computed several times, which especially raises the issue of computing the eigensolutions of a matrix pencil $(\mathbf{K}^s_{\mathtt{II}}, \mathbf{M}^s_{\mathtt{II}})$ several times, and computing the reduced matrices $\widetilde{\mathbf{M}}^s$ and $\widetilde{\mathbf{K}}^s$ several times (see Eq. (15)). For the sake of clarity, the numerical tasks which need to be repeated, as many times as the number of substructures considered, are listed hereafter:

(i) Computation of the Jacobian matrices $\mathbf{J}^{se}(\xi,\eta)$, and computation of the elementary matrices $\mathbf{M}^{se}$ and $\mathbf{K}^{se}$, see Eqs. (22) and (5);

(ii) Computation of the mass and stiffness matrices $\mathbf{M}^s$ and $\mathbf{K}^s$ of the substructures via assembly procedures of the elementary matrices $\mathbf{M}^{se}$ and $\mathbf{K}^{se}$, see Eq. (7);

(iii) Computation of the matrices of static modes and fixed interface modes $-(\mathbf{K}^s_{\mathtt{II}})^{-1}\mathbf{K}^s_{\mathtt{IB}}$ and $\widetilde{\mathbf{X}}^s$ of the substructures, and computation of the reduced matrices $\widetilde{\mathbf{M}}^s$ and $\widetilde{\mathbf{K}}^s$, see Eq. (15).

The computational load involved in the repetition of these numerical tasks linearly grows as a function of the number of substructures considered, and therefore, it may rapidly surpass that involved in the remaining tasks, i.e., (iv) assembly of the reduced mass and stiffness matrices $\widetilde{\mathbf{M}}^s$ and $\widetilde{\mathbf{K}}^s$ of the substructures together to build the FE model of a whole nearly periodic structure (Eq. (16)), and (v) resolution of the matrix equation (17).

A strategy is proposed in the next section which circumvents the issue of repeating, many times, the previous tasks (i-iii). In brief, this consists in computing the reduced matrices $\widetilde{\mathbf{M}}^s$ and $\widetilde{\mathbf{K}}^s$ for some particular distorted FE meshes which are obtained by considering particular "coordinates" $(\epsilon_x)_p$ and $(\epsilon_y)_p$ (see Eq. (21)), and approximating the reduced matrices between the resulting "interpolation points" $\widetilde{\mathbf{M}}_p$ and $\widetilde{\mathbf{K}}_p$ via appropriate interpolation functions.

3. Matrix interpolation

The proposed approach consists in computing a few number n^p of matrices $\widetilde{\mathbf{M}}_p$ and $\widetilde{\mathbf{K}}_p$ ($p = 1, 2, \ldots, n^p$) for some coordinates $\epsilon_x^s = (\epsilon_x)_p$ and $\epsilon_y^s = (\epsilon_y)_p$, and interpolating the matrix $\widetilde{\mathbf{M}}^s$ (resp. $\widetilde{\mathbf{K}}^s$) between the matrices $\widetilde{\mathbf{M}}_p$ (resp. $\widetilde{\mathbf{K}}_p$) for arbitrary ϵ_x^s and ϵ_y^s. The matrices $\widetilde{\mathbf{M}}_p$ and $\widetilde{\mathbf{K}}_p$ are expressed as follows, see Eqs. (13) and (15):

$$\widetilde{\mathbf{M}}_p = \widetilde{\mathbf{T}}_p^T \mathbf{M}_p \widetilde{\mathbf{T}}_p \quad , \quad \widetilde{\mathbf{K}}_p = \widetilde{\mathbf{T}}_p^T \mathbf{K}_p \widetilde{\mathbf{T}}_p, \tag{23}$$

where:

$$\widetilde{\mathbf{T}}_p = \begin{bmatrix} \mathbf{I}_{N_{\mathtt{B}}} & \mathbf{0} \\ -(\mathbf{K}_{\mathtt{II}})_p^{-1}(\mathbf{K}_{\mathtt{IB}})_p & \widetilde{\mathbf{X}}_p \end{bmatrix}. \tag{24}$$

Here, $-(\mathbf{K}_{\mathtt{II}})_p^{-1}(\mathbf{K}_{\mathtt{IB}})_p$ and $\widetilde{\mathbf{X}}_p$ are, respectively, the matrix of static modes and the reduced matrix of fixed interface modes obtained when $\epsilon_x^s = (\epsilon_x)_p$ and $\epsilon_y^s = (\epsilon_y)_p$. The number of fixed interface modes in $\widetilde{\mathbf{X}}_p$ is $M_{\mathtt{I}}$ (see before Eq. (11)) and is supposed to be identical for all the substructures.

The interest behind this interpolation strategy is that the matrices $\widetilde{\mathbf{M}}_p$ and $\widetilde{\mathbf{K}}_p$ are identical for all the substructures, i.e., they only need to be computed once. In other words, the previous tasks (i-iii) (see end of Sec. 2) can be highly reduced by computing a few number of matrices $\widetilde{\mathbf{M}}_p$ and $\widetilde{\mathbf{K}}_p$, only. The rest of the computational load concerns the computation of $\widetilde{\mathbf{M}}^s$ and $\widetilde{\mathbf{K}}^s$ via interpolation procedures, which is low-time consuming.

Although easy to understand, interpolating the matrix $\widetilde{\mathbf{M}}^s$ (resp. $\widetilde{\mathbf{K}}^s$) from matrices $\widetilde{\mathbf{M}}_p$ (resp. $\widetilde{\mathbf{K}}_p$) is not straightforward, however. The issue is that, despite the fact that the column ranges — i.e., the subspaces spanned by the column vectors — of the reduced matrices $\widetilde{\mathbf{X}}_p$ can be close to each other, their components may strongly differ, i.e., these reduced matrices are unable to describe any suitable interpolated matrix. This issue has been addressed in [18] where it is proposed to consider alternative reduced matrices $\widehat{\mathbf{X}}_p$ which are close to each other. This consists in considering a "common" matrix $\mathbf{\Psi}$ whose column range is close to those of $\widetilde{\mathbf{X}}_p$, and considering the projections of $\mathbf{\Psi}$ onto $\widetilde{\mathbf{X}}_p$ as new reduced matrices. This strategy can be understood as reordering and scaling the column vectors of $\widetilde{\mathbf{X}}_p$ to make them close to each other. These new reduced matrices are expressed by:

$$\widehat{\mathbf{X}}_p = \widetilde{\mathbf{X}}_p(\mathbf{\Psi}^T\widetilde{\mathbf{X}}_p)^{-1}\mathbf{\Psi}^T\mathbf{\Psi}. \tag{25}$$

Eq. (25) can be simplified when $\mathbf{\Psi}$ is orthogonal, i.e., $\mathbf{\Psi}^T\mathbf{\Psi} = \mathbf{I}$:

$$\widehat{\mathbf{X}}_p = \widetilde{\mathbf{X}}_p(\mathbf{\Psi}^T\widetilde{\mathbf{X}}_p)^{-1}. \tag{26}$$

Eq. (26) holds provided that the matrices $\mathbf{\Psi}^T\widetilde{\mathbf{X}}_p$ have full rank, which particularly means that the column ranges of the matrices $\widetilde{\mathbf{X}}_p$ have to be "sufficiently close" to the column range of the matrix $\mathbf{\Psi}$. This also means that the mesh distortions of the structures should be small enough, or in other words that the dispersion parameter δ of the random variables ϵ_x^s and ϵ_y^s (see Eq. (21)) has to be chosen in such a way that the matrices $\mathbf{\Psi}^T\widetilde{\mathbf{X}}_p$ have full rank.

In [18], it is proposed to consider the following Singular Value Decomposition (SVD) $[\widetilde{\mathbf{X}}_1\widetilde{\mathbf{X}}_2\cdots\widetilde{\mathbf{X}}_{n^p}] = \mathbf{U}\mathbf{\Sigma}\mathbf{V}^T$, and to define $\mathbf{\Psi}$ as the first $M_{\mathtt{I}}$ column vectors of $\mathbf{U}$ (i.e., the first $M_{\mathtt{I}}$ left singular vectors of the SVD). The underlying assumption behind this strategy is that the matrices $\widetilde{\mathbf{X}}_p$ must be orthogonal, which is not true in the present framework (i.e., they are orthogonal with respect to the mass matrix, but not in the usual sense, see comments about Eq. (10)). A different strategy is proposed here which consists in considering the following orthogonal matrix which concerns the fixed interface modes of the substructure with undistorted mesh ($\epsilon_x^s = 0$ and $\epsilon_y^s = 0$):

$$\mathbf{\Psi} = \left((\mathbf{M}^0_{\mathtt{II}})^{\frac{1}{2}}\right)^T \widetilde{\mathbf{X}}^0, \tag{27}$$

where notations $\mathbf{M}^0_{\mathtt{II}}$ and $\widetilde{\mathbf{X}}^0$ mean that the matrices $\mathbf{M}^s_{\mathtt{II}}$ (see Eq. (9)) and $\widetilde{\mathbf{X}}^s$ are expressed at coordinates $\epsilon_x^s = 0$ and $\epsilon_y^s = 0$. The fact that $\mathbf{\Psi}$ is an orthogonal matrix follows from Eq. (10).

By considering the new reduced matrices $\widehat{\mathbf{X}}_p$, this yields new transformation matrices $\widehat{\mathbf{T}}_p$ (see Eq. (13)) and new reduced mass and stiffness matrices $\widehat{\mathbf{M}}_p$ and $\widehat{\mathbf{K}}_p$, as follows:

$$\widehat{\mathbf{T}}_p = \begin{bmatrix} \mathbf{I}_{N_{\mathtt{B}}} & \mathbf{0} \\ -(\mathbf{K}_{\mathtt{II}})_p^{-1}(\mathbf{K}_{\mathtt{IB}})_p & \widehat{\mathbf{X}}_p \end{bmatrix}, \tag{28}$$

and

$$\widehat{\mathbf{M}}_p = \widehat{\mathbf{T}}_p^T\mathbf{M}_p\widehat{\mathbf{T}}_p \quad , \quad \widehat{\mathbf{K}}_p = \widehat{\mathbf{T}}_p^T\mathbf{K}_p\widehat{\mathbf{T}}_p. \tag{29}$$

Let us denote by $\widehat{\mathbf{M}}^s$ and $\widehat{\mathbf{K}}^s$ the interpolated reduced mass and stiffness matrices which result from arbitrary values of ϵ_x^s and ϵ_y^s with $-\delta \leq \epsilon_x^s \leq \delta$ and $-\delta \leq \epsilon_y^s \leq \delta$. They can be obtained as follows:

$$\widehat{\mathbf{M}}^s = \sum_{p=1}^{n^p} N_p(\xi^s, \eta^s)\widehat{\mathbf{M}}_p \quad , \quad \widehat{\mathbf{K}}^s = \sum_{p=1}^{n^p} N_p(\xi^s, \eta^s)\widehat{\mathbf{K}}_p, \tag{30}$$

where $N_p(\xi^s, \eta^s)$ are classical interpolation functions based on polynomials, while ξ^s and η^s are parametric coordinates. These can be chosen so that they are equal to -1 or 1 at "Tchebychev points" $-\delta/\sqrt{2}$ and $\delta/\sqrt{2}$, i.e.:

$$\xi^s = \sqrt{2}\frac{\epsilon_x^s}{\delta} \quad , \quad \eta^s = \sqrt{2}\frac{\epsilon_y^s}{\delta}. \tag{31}$$

Since $-\delta \leq \epsilon_x^s \leq \delta$ and $-\delta \leq \epsilon_y^s \leq \delta$, one has $-\sqrt{2} \leq \xi^s \leq \sqrt{2}$ and $-\sqrt{2} \leq \eta^s \leq \sqrt{2}$.

Here, an interpolation scheme based on eight interpolation points (ξ_p, η_p) and eight Serendipity interpolation functions [23] $N_p(\xi^s, \eta^s)$ is proposed, as illustrated in Fig. 4. Those interpolation points and interpolation functions are given by:

$$\begin{aligned}
(\xi_1, \eta_1) = (-1\,,\,-1) \quad , \qquad & N_1(\xi^s, \eta^s) = -\frac{1}{4}(1-\xi^s)(1-\eta^s)(1+\xi^s+\eta^s),\\
(\xi_2, \eta_2) = (1\,,\,-1) \quad , \qquad & N_2(\xi^s, \eta^s) = -\frac{1}{4}(1+\xi^s)(1-\eta^s)(1-\xi^s+\eta^s),\\
(\xi_3, \eta_3) = (1\,,\,1) \quad , \qquad & N_3(\xi^s, \eta^s) = -\frac{1}{4}(1+\xi^s)(1+\eta^s)(1-\xi^s-\eta^s),\\
(\xi_4, \eta_4) = (-1\,,\,1) \quad , \qquad & N_4(\xi^s, \eta^s) = -\frac{1}{4}(1-\xi^s)(1+\eta^s)(1+\xi^s-\eta^s),\\
(\xi_5, \eta_5) = (0\,,\,-1) \quad , \qquad & N_5(\xi^s, \eta^s) = \frac{1}{2}(1-\xi^s)(1+\xi^s)(1-\eta^s),\\
(\xi_6, \eta_6) = (1\,,\,0) \quad , \qquad & N_6(\xi^s, \eta^s) = \frac{1}{2}(1+\xi^s)(1-\eta^s)(1+\eta^s),\\
(\xi_7, \eta_7) = (0\,,\,1) \quad , \qquad & N_7(\xi^s, \eta^s) = \frac{1}{2}(1-\xi^s)(1+\xi^s)(1+\eta^s),\\
(\xi_8, \eta_8) = (-1\,,\,0) \quad , \qquad & N_8(\xi^s, \eta^s) = \frac{1}{2}(1-\xi^s)(1-\eta^s)(1+\eta^s).
\end{aligned} \tag{32}$$

The modeling of a whole nearly periodic structure, based on the interpolated matrices $\widehat{\mathbf{M}}^s$ and $\widehat{\mathbf{K}}^s$, follows as:

$$\left[(-\omega^2 + \mathtt{i}\omega a)\widehat{\mathbf{M}}_{\mathtt{per}} + (\mathtt{i}\omega b + 1)\widehat{\mathbf{K}}_{\mathtt{per}}\right]\begin{bmatrix}(\widehat{\mathbf{u}}_{\mathtt{B}})_{\mathtt{per}}\\ \widehat{\boldsymbol{\alpha}}_{\mathtt{per}}\end{bmatrix} = \widehat{\mathbf{F}}_{\mathtt{per}}, \tag{33}$$

where (see Eq. (16)):

$$\widehat{\mathbf{M}}_{\mathtt{per}} = \sum_s (\widetilde{\mathbf{L}}^s)^T \widehat{\mathbf{M}}^s \widetilde{\mathbf{L}}^s \quad , \quad \widehat{\mathbf{K}}_{\mathtt{per}} = \sum_s (\widetilde{\mathbf{L}}^s)^T \widehat{\mathbf{K}}^s \widetilde{\mathbf{L}}^s. \tag{34}$$

In Eq. (33), $(\widehat{\mathbf{u}}_{\mathtt{B}})_{\mathtt{per}}$ is the displacement vector of the boundary/interface nodes of the substructures (i.e., that obtained by considering the interpolated matrices) and $\widehat{\boldsymbol{\alpha}}_{\mathtt{per}} = [(\widehat{\boldsymbol{\alpha}}^1)^T(\widehat{\boldsymbol{\alpha}}^2)^T \cdots]^T$ is the vector of generalized coordinates (see Eq. (18)). The force vector $\widehat{\mathbf{F}}_{\mathtt{per}}$ in Eq. (33) is expressed from the local force vectors of the substructures which can be interpolated in the same way as $\widehat{\mathbf{M}}^s$ and $\widehat{\mathbf{K}}^s$ (see Eqs. (30) and (18)), i.e.:

$$\widehat{\mathbf{F}}_{\mathtt{per}} = \sum_s (\widetilde{\mathbf{L}}^s)^T \widehat{\mathbf{F}}^s, \tag{35}$$

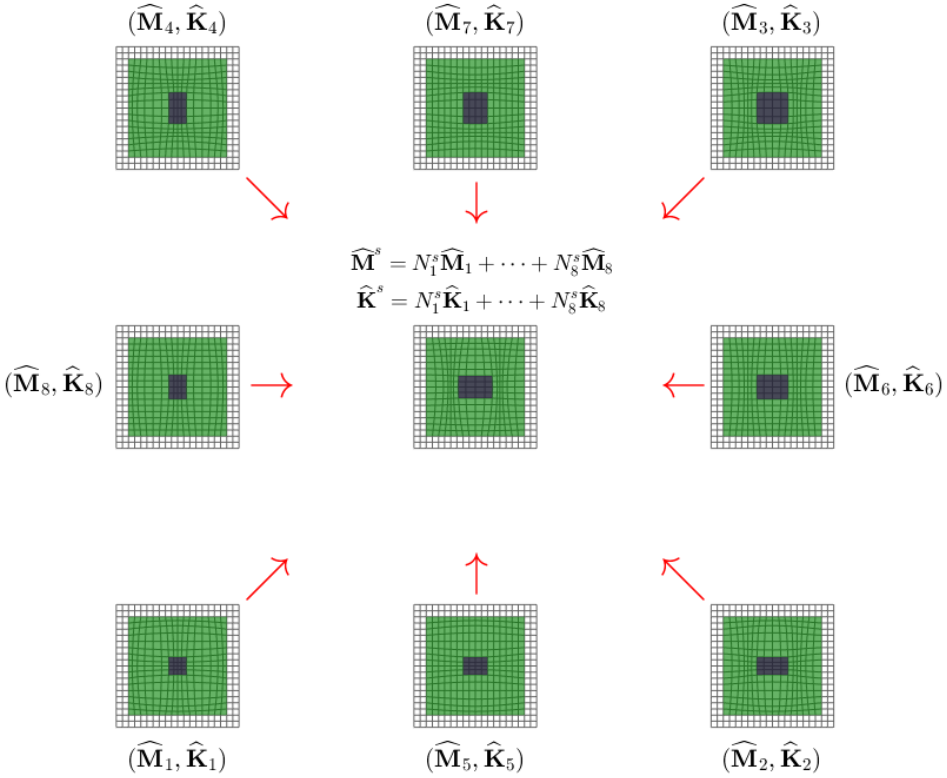

Figure 4: Eight point interpolation scheme based on serendipity interpolation functions $N_p(\xi^s, \eta^s)$ $(p = 1, \ldots, 8)$.

where

$$\widehat{\mathbf{F}}^s = \sum_{p=1}^{8} N_p(\xi^s, \eta^s) \widehat{\mathbf{F}}_p^s, \tag{36}$$

and

$$\widehat{\mathbf{F}}_p^s = \begin{bmatrix} \mathbf{F}_{\mathtt{B}}^s - (\mathbf{K}_{\mathtt{BI}})_p (\mathbf{K}_{\mathtt{II}})_p^{-1} \mathbf{F}_{\mathtt{I}}^s \\ \widehat{\mathbf{X}}_p^T \mathbf{F}_{\mathtt{I}}^s \end{bmatrix}. \tag{37}$$

The expression of $\widehat{\mathbf{F}}^s$ can be strongly simplified when $\mathbf{F}_{\mathtt{I}}^s = \mathbf{0}$, i.e., by assuming that the internal nodes of the substructures are free from excitations. This yields:

$$\widehat{\mathbf{F}}^s = \begin{bmatrix} \mathbf{F}_{\mathtt{B}}^s \\ \mathbf{0} \end{bmatrix} \qquad \text{when} \quad \mathbf{F}_{\mathtt{I}}^s = \mathbf{0}. \tag{38}$$

Solving Eq. (33) yields the displacement vector of the boundary nodes $(\widehat{\mathbf{u}}_{\mathtt{B}})_{\mathtt{per}}$ and the vector of generalized coordinates $\widehat{\boldsymbol{\alpha}}_{\mathtt{per}}$. In addition, the displacement vectors of the internal nodes of the substructures — namely, $\widehat{\mathbf{u}}_{\mathtt{I}}^s$ — may be easily obtained as follows:

$$\widehat{\mathbf{u}}_{\mathtt{I}}^s \approx -(\mathbf{K}_{\mathtt{II}}^0)^{-1} \mathbf{K}_{\mathtt{IB}}^0 \widehat{\mathbf{u}}_{\mathtt{B}}^s + \widehat{\mathbf{X}}^0 \widehat{\boldsymbol{\alpha}}^s, \tag{39}$$

where $-(\mathbf{K}^0_{\mathtt{II}})^{-1}\mathbf{K}^0_{\mathtt{IB}}$ is the matrix of static modes when $\epsilon^s_x = 0$ and $\epsilon^s_y = 0$ (undistorted mesh), while matrix $\widehat{\mathbf{X}}^0$ is given by $\widehat{\mathbf{X}}^0 = \widetilde{\mathbf{X}}^0(\boldsymbol{\Psi}^T\widetilde{\mathbf{X}}^0)^{-1}$ (see Eq. (26)). Also, $\widehat{\mathbf{u}}^s_{\mathtt{B}}$ denotes the displacement vectors of the boundary nodes of the substructures, expressed by $\widehat{\mathbf{u}}^s_{\mathtt{B}} = \widetilde{\mathbf{L}}^s_{\mathtt{B}}(\widehat{\mathbf{u}}_{\mathtt{B}})_{\mathtt{per}}$ where $\widetilde{\mathbf{L}}^s_{\mathtt{B}}$ are the localization matrices introduced earlier after Eq. (20).

The procedure for modeling an assembly made up of different nearly periodic structures — i.e., whose related substructures have different material properties and are described with FE meshes whose distortions are governed in different ways — and different (purely) periodic structures, with mass, stiffness and damping matrices $\widehat{\mathbf{M}}^u_{\mathtt{per}}$, $\widehat{\mathbf{K}}^u_{\mathtt{per}}$ and $\widehat{\mathbf{C}}^u_{\mathtt{per}}$ ($u = 1, 2, \ldots$) follows from FE assembly procedures. In this case, the mass, stiffness and damping matrices of the assembly — namely, $\widehat{\mathbf{M}}_{\mathtt{a}}$, $\widehat{\mathbf{K}}_{\mathtt{a}}$ and $\widehat{\mathbf{C}}_{\mathtt{a}}$ — are obtained as follows:

$$\widehat{\mathbf{M}}_{\mathtt{a}} = \sum_u (\widehat{\mathbf{L}}^u_{\mathtt{per}})^T \widehat{\mathbf{M}}^u_{\mathtt{per}} \widehat{\mathbf{L}}^u_{\mathtt{per}}, \tag{40}$$

$$\widehat{\mathbf{K}}_{\mathtt{a}} = \sum_u (\widehat{\mathbf{L}}^u_{\mathtt{per}})^T \widehat{\mathbf{K}}^u_{\mathtt{per}} \widehat{\mathbf{L}}^u_{\mathtt{per}}, \tag{41}$$

and

$$\widehat{\mathbf{C}}_{\mathtt{a}} = \sum_u (\widehat{\mathbf{L}}^u_{\mathtt{per}})^T \left(a^u_{\mathtt{per}} \widehat{\mathbf{M}}^u_{\mathtt{per}} + b^u_{\mathtt{per}} \widehat{\mathbf{K}}^u_{\mathtt{per}} \right) \widehat{\mathbf{L}}^u_{\mathtt{per}}, \tag{42}$$

where $a^u_{\mathtt{per}}$ and $b^u_{\mathtt{per}}$ are damping coefficients (see Eq. (2)), while $\widehat{\mathbf{L}}^u_{\mathtt{per}}$ are localization matrices. In this case, the dynamic equilibrium equation is written as:

$$\left[-\omega^2 \widehat{\mathbf{M}}_{\mathtt{a}} + \mathtt{i}\omega \widehat{\mathbf{C}}_{\mathtt{a}} + \widehat{\mathbf{K}}_{\mathtt{a}} \right] \begin{bmatrix} (\widehat{\mathbf{u}}_{\mathtt{B}})_{\mathtt{a}} \\ \widehat{\boldsymbol{\alpha}}_{\mathtt{a}} \end{bmatrix} = \widehat{\mathbf{F}}_{\mathtt{a}}, \tag{43}$$

where $(\widehat{\mathbf{u}}_{\mathtt{B}})_{\mathtt{a}}$ is the displacement vector of the boundary/interface nodes of the substructures, and where $\widehat{\boldsymbol{\alpha}}_{\mathtt{a}} = [(\widehat{\boldsymbol{\alpha}}^1_{\mathtt{per}})^T (\widehat{\boldsymbol{\alpha}}^2_{\mathtt{per}})^T \cdots]^T$. Also, the BCs of the assembly can be expressed in the same way as Eq. (19).

The matrix system (43) is similar to that obtained with the classical CB method (i.e., same size and same matrix structure). However, the CPU times required by the computation of the matrices $\widehat{\mathbf{M}}_{\mathtt{a}}$, $\widehat{\mathbf{K}}_{\mathtt{a}}$ and $\widehat{\mathbf{C}}_{\mathtt{a}}$ are much lower with the interpolation strategy (see discussion at the end of Sec. 2). Indeed, recall that the proposed strategy requires, for a given nearly periodic structure, the computation of eight reduced mass matrices $\widehat{\mathbf{M}}_p$ and eight reduced stiffness matrices $\widehat{\mathbf{K}}_p$, that's it! Those are used to determine (via interpolation) the reduced mass and stiffness matrices $\widehat{\mathbf{M}}^s$ and $\widehat{\mathbf{K}}^s$ of all the substructures, whatever the values of the random variables ϵ^s_x and ϵ^s_y (see Eq. (21)).

A second reduced mode expansion (i.e., in addition to that considered for modeling the substructures) can be proposed to speed up the computation of the matrix system (43). This second model reduction is detailed as follows. Let us rewrite, first, the mass, stiffness and damping matrices of the assembly as follows:

$$\widehat{\mathbf{M}}_{\mathtt{a}} = \begin{bmatrix} (\widehat{\mathbf{M}}_{\mathtt{BB}})_{\mathtt{a}} & (\widehat{\mathbf{M}}_{\mathtt{B}\alpha})_{\mathtt{a}} \\ (\widehat{\mathbf{M}}_{\alpha\mathtt{B}})_{\mathtt{a}} & (\widehat{\mathbf{M}}_{\alpha\alpha})_{\mathtt{a}} \end{bmatrix} \quad , \quad \widehat{\mathbf{K}}_{\mathtt{a}} = \begin{bmatrix} (\widehat{\mathbf{K}}_{\mathtt{BB}})_{\mathtt{a}} & (\widehat{\mathbf{K}}_{\mathtt{B}\alpha})_{\mathtt{a}} \\ (\widehat{\mathbf{K}}_{\alpha\mathtt{B}})_{\mathtt{a}} & (\widehat{\mathbf{K}}_{\alpha\alpha})_{\mathtt{a}} \end{bmatrix} \quad , \quad \widehat{\mathbf{C}}_{\mathtt{a}} = \begin{bmatrix} (\widehat{\mathbf{C}}_{\mathtt{BB}})_{\mathtt{a}} & (\widehat{\mathbf{C}}_{\mathtt{B}\alpha})_{\mathtt{a}} \\ (\widehat{\mathbf{C}}_{\alpha\mathtt{B}})_{\mathtt{a}} & (\widehat{\mathbf{C}}_{\alpha\alpha})_{\mathtt{a}} \end{bmatrix}. \tag{44}$$

Also, let us define by $\widehat{\mathbf{M}}^0_{\mathtt{a}}$ and $\widehat{\mathbf{K}}^0_{\mathtt{a}}$ the mass and stiffness matrices obtained when $\epsilon^s_x = 0$ and $\epsilon^s_y = 0$ for all the substructures (periodic case), and let us express the displacement vector $(\widehat{\mathbf{u}}_{\mathtt{B}})_{\mathtt{a}}$ as follows:

$$(\widehat{\mathbf{u}}_{\mathtt{B}})_{\mathtt{a}} = \widetilde{\mathbf{X}}^0_{\mathtt{a}} \widetilde{\boldsymbol{\beta}}_{\mathtt{a}}, \tag{45}$$

where $\widetilde{\mathbf{X}}^0_{\mathtt{a}} = [(\boldsymbol{\chi}^0_{\mathtt{a}})_1 (\boldsymbol{\chi}^0_{\mathtt{a}})_2 \cdots (\boldsymbol{\chi}^0_{\mathtt{a}})_{M_{\mathtt{a}}}]$ is a reduced matrix of modes $(\boldsymbol{\chi}^0_{\mathtt{a}})_j$ ($j = 1, 2, \ldots, M_{\mathtt{a}}$) which represent the first $M_{\mathtt{a}}$ eigenvectors of the matrix pencil $\left((\widehat{\mathbf{K}}_{\mathtt{BB}})^0_{\mathtt{a}}, (\widehat{\mathbf{M}}_{\mathtt{BB}})^0_{\mathtt{a}} \right)$. Notice that these modes do not depend on the random variables ϵ^s_x and ϵ^s_y, i.e., they only need to be computed once.

Then, define the transformation matrix $\widetilde{\mathbf{T}}_{\mathtt{a}}^{0}$, defined so that:

$$\begin{bmatrix} (\widehat{\mathbf{u}}_{\mathtt{B}})_{\mathtt{a}} \\ \widehat{\boldsymbol{\alpha}}_{\mathtt{a}} \end{bmatrix} = \widetilde{\mathbf{T}}_{\mathtt{a}}^{0} \begin{bmatrix} \widetilde{\boldsymbol{\beta}}_{\mathtt{a}} \\ \widehat{\boldsymbol{\alpha}}_{\mathtt{a}} \end{bmatrix}, \tag{46}$$

where

$$\widetilde{\mathbf{T}}_{\mathtt{a}}^{0} = \begin{bmatrix} \widetilde{\mathbf{X}}_{\mathtt{a}}^{0} & \mathbf{0} \\ \mathbf{0} & \mathbf{I} \end{bmatrix}. \tag{47}$$

As a result, the following reduced matrix system, with reduced matrices $[(\widetilde{\mathbf{T}}_{\mathtt{a}}^{0})^{T}\widehat{\mathbf{M}}_{\mathtt{a}}\widetilde{\mathbf{T}}_{\mathtt{a}}^{0}]$, $[(\widetilde{\mathbf{T}}_{\mathtt{a}}^{0})^{T}\widehat{\mathbf{C}}_{\mathtt{a}}\widetilde{\mathbf{T}}_{\mathtt{a}}^{0}]$ and $[(\widetilde{\mathbf{T}}_{\mathtt{a}}^{0})^{T}\widehat{\mathbf{K}}_{\mathtt{a}}\widetilde{\mathbf{T}}_{\mathtt{a}}^{0}]$, can be proposed:

$$\left[-\omega^{2}[(\widetilde{\mathbf{T}}_{\mathtt{a}}^{0})^{T}\widehat{\mathbf{M}}_{\mathtt{a}}\widetilde{\mathbf{T}}_{\mathtt{a}}^{0}] + \mathtt{i}\omega[(\widetilde{\mathbf{T}}_{\mathtt{a}}^{0})^{T}\widehat{\mathbf{C}}_{\mathtt{a}}\widetilde{\mathbf{T}}_{\mathtt{a}}^{0}] + [(\widetilde{\mathbf{T}}_{\mathtt{a}}^{0})^{T}\widehat{\mathbf{K}}_{\mathtt{a}}\widetilde{\mathbf{T}}_{\mathtt{a}}^{0}]\right] \begin{bmatrix} \widetilde{\boldsymbol{\beta}}_{\mathtt{a}} \\ \widehat{\boldsymbol{\alpha}}_{\mathtt{a}} \end{bmatrix} = (\widetilde{\mathbf{T}}_{\mathtt{a}}^{0})^{T}\widehat{\mathbf{F}}_{\mathtt{a}}. \tag{48}$$

Eventually, a last model reduction based on a reduced set of eigenvectors of $\left([(\widetilde{\mathbf{T}}_{\mathtt{a}}^{0})^{T}\widehat{\mathbf{K}}_{\mathtt{a}}\widetilde{\mathbf{T}}_{\mathtt{a}}^{0}], [(\widetilde{\mathbf{T}}_{\mathtt{a}}^{0})^{T}\widehat{\mathbf{M}}_{\mathtt{a}}\widetilde{\mathbf{T}}_{\mathtt{a}}^{0}]\right)$ can be proposed to further reduce the size of the matrix system. This computational task is not expensive given that the size of $[(\widetilde{\mathbf{T}}_{\mathtt{a}}^{0})^{T}\widehat{\mathbf{K}}_{\mathtt{a}}\widetilde{\mathbf{T}}_{\mathtt{a}}^{0}]$ and $[(\widetilde{\mathbf{T}}_{\mathtt{a}}^{0})^{T}\widehat{\mathbf{M}}_{\mathtt{a}}\widetilde{\mathbf{T}}_{\mathtt{a}}^{0}]$ is not large. Note that this model reduction can be used to analyze of single nearly periodic structure. In this case, one has $\widehat{\mathbf{M}}_{\mathtt{a}} = \widehat{\mathbf{M}}_{\mathtt{per}}$ and $\widehat{\mathbf{K}}_{\mathtt{a}} = \widehat{\mathbf{K}}_{\mathtt{per}}$.

4. Numerical results

4.1. Preliminary comments

The efficiency of the interpolation strategy proposed in Sec. 3 is discussed. For this purpose, three structures are analyzed which concern: (1) a nearly periodic plate with 8×8 substructures (Fig. 5), (2) a nearly periodic plate with 15×15 substructures (Fig. 9) and (3) an assembly consisting in a nearly periodic plate with 8×4 substructures embedded in a floor panel (Fig. 14). Regarding the floor panel, it is modeled with homogeneous substructures of same dimensions as those used to model the nearly periodic plates.

The first test case involves a nearly periodic plate with 64 substructures and about $230,000$ DOFs. The second test case involves 225 substructures and more than $800,000$ DOFs, and is proposed here with a view to demonstrating the potential of the model reduction strategy to handle moderately large-sized FE models. The third test case involves a nearly periodic plate embedded in a floor panel and intends to highlight the dynamic behavior of assemblies made up of regular structures (floor) coupled to resonant metamaterials (plate), which is of interest for engineering applications.

Especially, the harmonic response of each structure is analyzed over a frequency band of $[0\,,\,150]$ Hz. The plates/substructures are meshed using eight-node isoparametric Mindlin plate elements, with three DOFs per node, whose mass and stiffness matrices are given in Appendix (see also [24, 25]). The computation of these matrices is performed via Gauss point quadrature using 3×3 Gauss points. A schematic of a substructure with a distorted mesh is given in Fig. 3. It is of square shape with global dimensions $L_x = L = 0.25$ m and $L_y = L = 0.25$ m (width and height), thickness of 0.005 m, and it is composed of an external layer in steel (in gray color), a medium layer in rubber (in green color), and a core in tungsten (in black color). The related material properties are given in Tab. 1. Also, it is meshed using 20×20 elements — leading to 3843 DOFs with 480 boundary DOFs — which is supposed to be high enough to accurately describe the displacement fields within $[0\,,\,150]$ Hz. The expression of the damping matrix of the substructures follows from Eq. (2), where $a = 5 \times 10^{-3}$ s^{-1} and $b = 2 \times 10^{-6}$ s.

The external layers of the substructures are supposed to be part of a global frame structure (in steel) whose dimensions are fixed by design purposes and which contains several inclusions filled with rubber and tungsten parts. In other words, these are the two parts whose geometrical properties vary between the substructures, and

which are modeled with a distorted mesh (see Fig. 3). The latter is obtained following Eq. (21) where functions $f_x(x_j^e, y_j^e)$ and $f_y(x_j^e, y_j^e)$ are defined such that:

$$f_x(x_j^e, y_j^e) = 0 \quad \text{and} \quad f_y(x_j^e, y_j^e) = 0 \qquad \text{when} \;\; x_j^e \leq L_{\texttt{st}} \;,\; y_j^e \leq L_{\texttt{st}} \;,\; x_j^e \geq (L - L_{\texttt{st}}) \;\; \text{or} \;\; y_j^e \geq (L - L_{\texttt{st}}), \tag{49}$$

$$f_x(x_j^e, y_j^e) = \sin\left[\frac{4\pi(x_j^e - L_{\texttt{st}})}{L - 2L_{\texttt{st}}}\right] \sin\left[\frac{\pi(y_j^e - L_{\texttt{st}})}{L - 2L_{\texttt{st}}}\right] \qquad \text{when} \;\; L_{\texttt{st}} \leq x_j^e \leq (L - L_{\texttt{st}}) \;\; \text{and} \;\; L_{\texttt{st}} \leq y_j^e \leq (L - L_{\texttt{st}}), \tag{50}$$

$$f_y(x_j^e, y_j^e) = \sin\left[\frac{4\pi(y_j^e - L_{\texttt{st}})}{L - 2L_{\texttt{st}}}\right] \sin\left[\frac{\pi(x_j^e - L_{\texttt{st}})}{L - 2L_{\texttt{st}}}\right] \qquad \text{when} \;\; L_{\texttt{st}} \leq x_j^e \leq (L - L_{\texttt{st}}) \;\; \text{and} \;\; L_{\texttt{st}} \leq y_j^e \leq (L - L_{\texttt{st}}), \tag{51}$$

where $L_{\texttt{st}} = 0.025$ m is the width of the external layer. The random variables used to generate the distorted mesh are ϵ_x^s and ϵ_y^s (see Eq. (21)), and follow a uniform probability law with a dispersion of $\delta = 0.01$ m. Such a distorted mesh is shown for the substructure displayed in Fig. 3 where $\epsilon_x^s = -0.0094$ m and $\epsilon_y^s = 0.0089$ m.

Concerning the CB modeling of the substructures, a number of $M_{\texttt{I}} = 5$ fixed interface modes — with eigenfrequencies $f_1 = 46.74$ Hz, $f_2 = 135.16$ Hz, $f_3 = 135.16$ Hz, $f_4 = 367.11$ Hz and $f_5 = 374.03$ Hz — are used. The strategy for selecting these modes is classical and consists in selecting the modes whose eigenfrequencies are below two or three times the maximum frequency of the frequency band analyzed (150 Hz here).

Table 1: Material properties of the substructures.

	Density (kg.m^{-3})	Young's modulus (GPa)	Poisson's ratio
Steel (external layer):	7850	220	0.3
Rubber (medium layer):	950	0.15	0.48
Tungsten (core):	19, 250	340	0.27

Numerical simulations are carried out using MATLAB and in-house implementations of the proposed approaches. For each structure analyzed, the displacement solution obtained with the interpolation strategy is compared to the result issued from the FE method. The latter involves assembling many eight-node plate elements to build the global mass and stiffness matrices of the plates (and the floor). These global matrices are sparse, and as such, they can be quickly generated via appropriate procedure. In the present case, the procedure proposed in [26], well suited for MATLAB, is used. As for the interpolation strategy, the assembly of the mass and stiffness matrices of the substructures is also undertaken with the procedure proposed in [26]. In order to propose a fair comparison between the interpolation strategy and the FE method, for each structure analyzed, a global model reduction similar to that proposed at the end of Sec. 3, based on a same number of modes, is applied to both the interpolation-based model and the FE model.

Additional results are presented which are issued from the CB method. This involves considering the numerical tasks (i-iii) listed at the end of Sec. 2 for every substructure considered. Especially, the computational times involved in the CB method are highlighted and compared to those involved in the interpolation strategy and the FE method.

Recall that the key advantage of the interpolation strategy is to overcome the issue of considering several cumbersome numerical tasks for modeling substructures with different distorted meshes. Instead, the strategy

requires a few "offline" tasks — i.e., the computation of reduced mass and stiffness matrices at eight interpolation points — which only need to be performed once, i.e., regardless of the distorted mesh considered. These offline tasks are cheap and, since they do not need to be repeated for modeling the substructures, they will not be considered in the assessment of the computational times presented below. Besides, the reduced matrix $\widetilde{\mathbf{X}}_{\mathtt{a}}^{0}$ in Eq. (47) only needs to be computed once and for all, regardless of the distorted mesh and dispersion δ considered; therefore, the computational time required to calculate this matrix will not be reported hereafter.

For the sake of clarity, a summary of the numerical tasks required by the FE method, the interpolation strategy and the CB method are given hereafter:

- **FE method:**
  (i) Structure (plate with or without floor) modeling via element assembly, and (ii) global model reduction (reduced mass and stiffness matrices) based on the eigenvectors of the stiffness and mass matrices of the structure (see end of Sec. 3).

- **Interpolation strategy:**
  (i) Substructure modeling via interpolation strategy, (ii) structure modeling via substructure assembly, (iii) model reduction based on Eq. (48), and (iv) global model reduction (see end of Sec. 3).

- **CB method:**
  (i) Substructure modeling via element assembly and CB method, (ii) structure modeling via substructure assembly, (iii) model reduction based on Eq. (48), and (iv) global model reduction (see end of Sec. 3).

An overview of the numerical models and computational times involved in the FE method and interpolation strategy is given in Tab. 2.

Table 2: Overview of the numerical models and numerical results.

	FE (reference)			Interpolated		
	Plate 1 (Fig. 5)	Plate 2 (Fig. 9)	Plate + floor (Fig. 14)	Plate 1 (Fig. 5)	Plate 2 (Fig. 9)	Plate + floor (Fig. 14)
DOFs:	$231,043$	$811,203$	$461,763$	$16,131$	$55,653$	$31,939$
DOFs (Eq. (48)):	—	—	—	$400+64\times5$	$1100+225\times5$	$400+128\times5$
DOFs (global reduction):	300	800	200	300	800	200
Time reduction:	—	—	—	86%	89%	82%

4.2. Nearly periodic plate with 8×8 *substructures*

A nearly periodic plate with 8×8 substructures, simply supported along its edges and subject to a point harmonic force (input), is considered as shown in Fig. 5. Especially, the variation of the quadratic velocity measured at some point (output) — defined by $\omega^2|w_{\mathtt{out}}|^2$ where $w_{\mathtt{out}}$ denotes the transverse displacement — is assessed over the frequency band $[0\,,\,150]$ Hz. The related frequency response function (FRF) $\omega\mapsto\omega^2|w_{\mathtt{out}}|^2$, computed with the FE method, is shown in Fig. 6 along with the FRF of the (purely) periodic plate, i.e., without distorted meshes. Also, the solution issued from the interpolation strategy, for the nearly periodic plate, is shown in Fig. 6.

About the periodic case, two band gaps occur which represent frequency bands on which the quadratic velocity levels are highly reduced. Band gaps are due to local resonances, within the substructures, and occur close to the fixed interface modes of the substructures (see dotted vertical red lines in Fig. 6). It is shown that, for frequencies less than 100 Hz and around the first band gap, the dynamic behavior of the nearly periodic plate is roughly similar to that of the periodic plate. Differences occur at higher frequencies which show an overall reduction of the displacement/quadratic velocity levels of the nearly periodic structure, except around the second band gap. Notice that the FRF issued from the interpolation strategy closely matches the FE solution over the whole frequency band, which gives credit to the proposed approach.

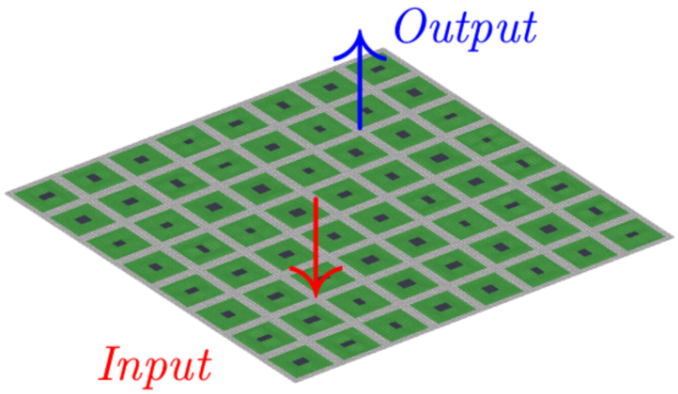

Figure 5: Schematic of a nearly periodic plate with 8×8 substructures and subject to a point harmonic force.

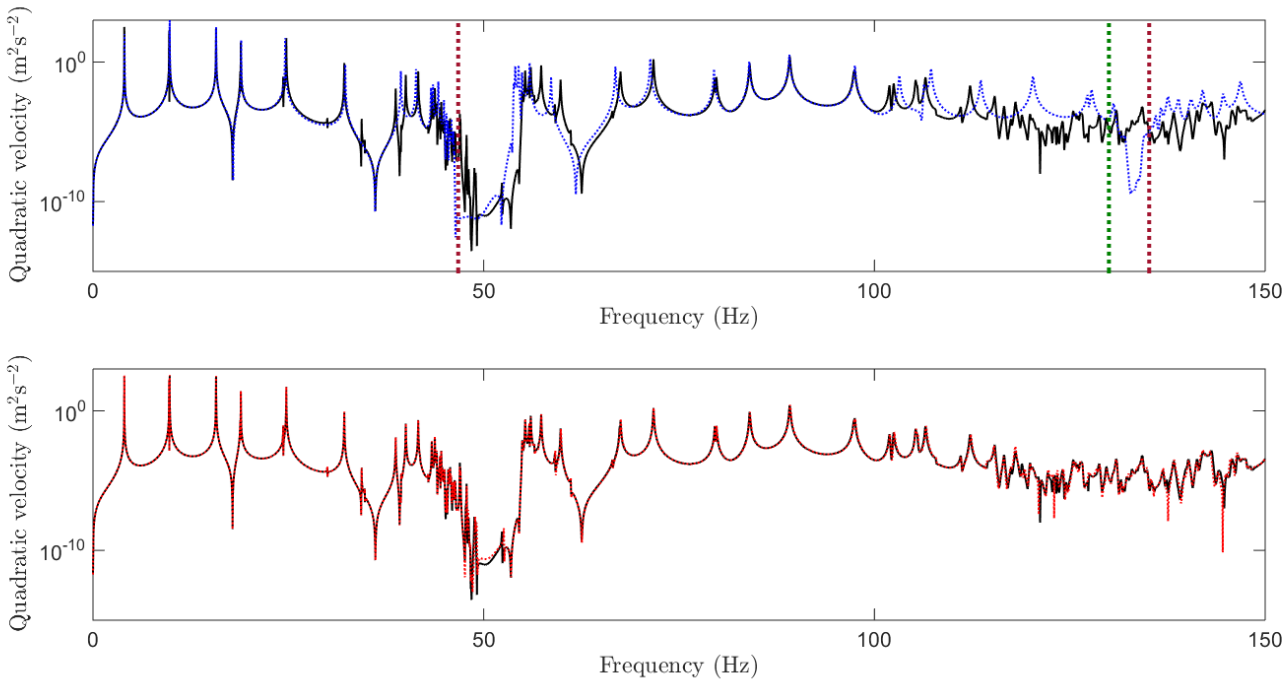

Figure 6: FRF (quadratic velocity) of the plate with 8×8 substructures. (black solid line) FE method, nearly periodic structure; (red dotted line) interpolation strategy, nearly periodic structure; (blue dotted line) FE method, purely periodic structure.

Also, the transverse displacement field of the plate can be assessed via the interpolation strategy. This involves computing the displacement vector of the boundary/interface nodes of the substructures by means of Eqs. (48) and (46), and expressing the displacement vectors of the internal nodes of the substructures with Eq. (39). Results are shown in Fig. 7 for the displacement fields of the periodic plate and the nearly periodic one, at a frequency of 130 Hz (see dotted vertical green line in Fig. 6). These results show that, when compared to the periodic case, the displacement field of the nearly periodic structure exhibits high levels around the excitation point, and low levels elsewhere. This seems to be in agreement with the literature [1]. Here again, the solution issued from the proposed approach closely matches the FE result as shown in Fig. 8.

An overview of the numerical models involved in the FE method and the interpolation strategy is given in Tab. 2. Recall that, within the framework of the interpolation strategy, $M_{\mathrm{I}} = 5$ fixed interface modes are used for modeling each substructure. Also, the displacement vector of the boundary/interface nodes of the

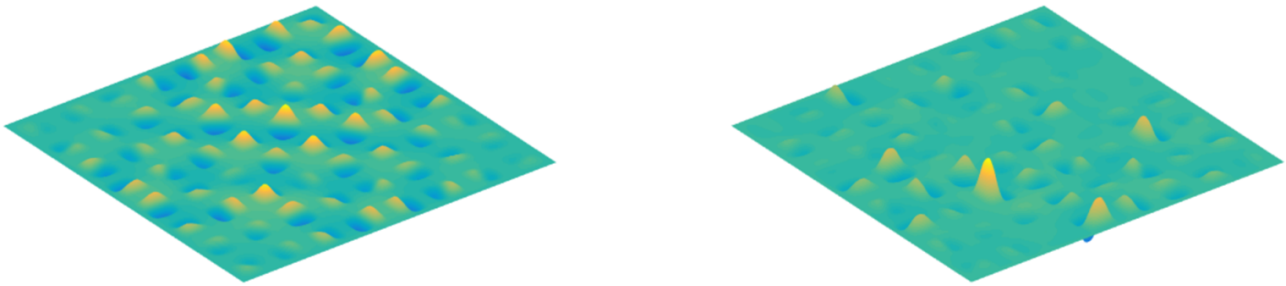

Figure 7: Transverse displacement field (real part) of the plate with 8×8 substructures at 130 Hz, obtained with the interpolation strategy. (left) Periodic case; (right) nearly periodic case.

substructures are expressed by means of $M_{\mathtt{a}} = 400$ modes $(\boldsymbol{\chi}_{\mathtt{a}}^0)_j$, see Eq. (45). This yields $400 + 8^2 \times 5$ DOFs for the whole model. Finally, a global model reduction with 300 modes is considered as explained in Sec. 4.1. The choice of these numbers of modes — i.e., $M_{\mathtt{a}} = 400$ and 300 (global reduction) — is determined through a sensitivity analysis of the FRF(s) at high frequencies. As for the FE method, a global model reduction with a same number of modes (300) is also considered. The computational loads required for computing the FRFs of the plate using those global (FE-based and interpolation-based) reduced models, with 300 DOFs, are similar and small. Actually, the main computational burden comes from the computation of the reduced models. To achieve this task, the interpolation strategy appears to be clearly advantageous with a time reduction of 86% compared to the FE method.

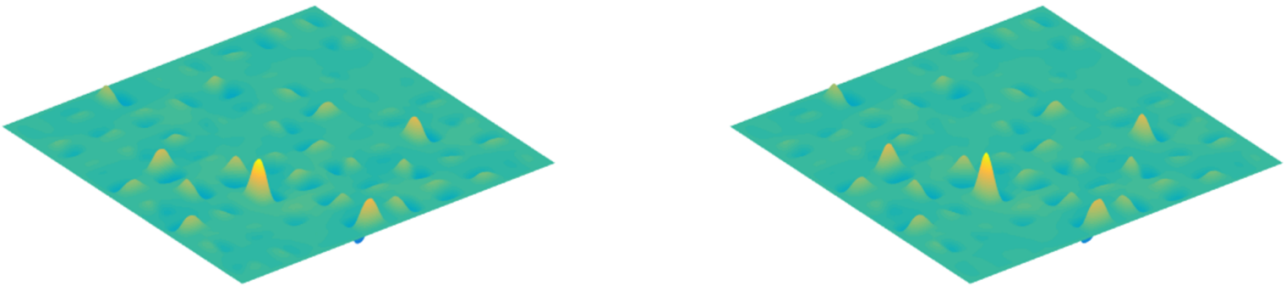

Figure 8: Transverse displacement field (real part) of the nearly periodic plate with 8×8 substructures at 130 Hz. (left) Interpolation strategy; (right) FE method.

In addition, the classical CB method can be considered, as explained earlier. The related FRF (not shown here) is similar to that obtained with the FE method. The computational burden of the CB method is mostly linked to the modeling of the substructures (numerical tasks (i-iii) listed at the end of Sec. 2). In this case, the time required for computing the reduced model of the plate (300 DOFs) exceeds that involved in the FE method, and therefore, that involved in the interpolation strategy. As a second shortcoming of the CB method, it fails to describe the displacement vectors of the internal nodes of the substructures via Eq. (39). This issue is linked to the fact that the matrices of fixed interface modes of the substructures $\widetilde{\mathbf{X}}^s$ can strongly differ from $\widehat{\mathbf{X}}^0$ (see Sec. 3 for further discussions).

4.3. Nearly periodic plate with 15×15 *substructures*

To further highlight the efficiency of the interpolation strategy, a second plate with 15×15 substructures is analyzed as shown in Fig. 9. Again, the plate is simply supported along its edges and is subject to a point harmonic force. In this case, the number of DOFs involved in the full FE model of the structure is $811,203$ which is moderately high (see Tab. 2 for the DOFs involved in the interpolation strategy). The FRF (quadratic

velocity) of the nearly periodic plate is shown in Fig. 10 along with that of the periodic plate. For the sake of clarity, the FRFs are displayed on the frequency band $[75\ ,\ 150]$ Hz, i.e., where differences between the periodic and nearly periodic structures are likely to occur. Again, the displacement levels of the nearly periodic plate undergo an overall reduction compared to the periodic case. For instance, the transverse displacement fields of the periodic and nearly periodic plates at 125 Hz (see dotted vertical green line in Fig. 10) are shown in Fig. 11 where it is observed that the vibrational energy of the nearly periodic structure is confined around the excitation point.

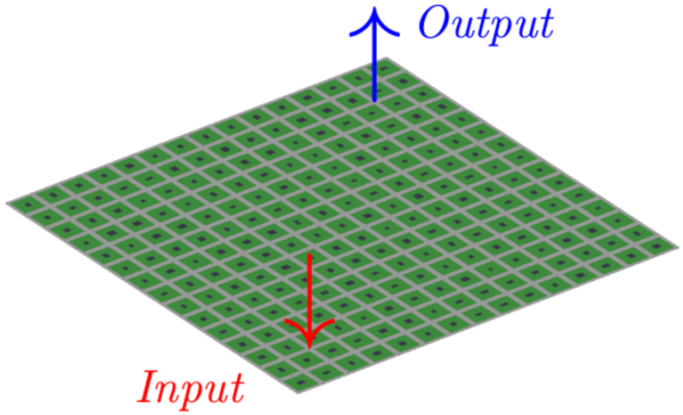

Figure 9: Schematic of a nearly periodic plate with 15×15 substructures and subject to a point harmonic force.

Again, the FRF and the displacement field obtained by means of the interpolation strategy approximate well the FE solutions (see Figs. 10 and 12). Here, the displacement vector of the boundary/interface nodes of the substructures are expressed by means of $M_{\mathtt{a}} = 1100$ modes $(\boldsymbol{\chi}_{\mathtt{a}}^0)_j$ (see Eq. (45)), leading to $1100 + 15^2 \times 5$ DOFs for the interpolation-based model. A global model reduction is also considered (see Sec. 4.1) for both the interpolation strategy and the FE method which involves 800 modes. In this case again, the computation of the reduced model of the nearly periodic plate is significantly sped up with the interpolation strategy, i.e., 89% time saving compared to the FE method. In contrast, the classical CB method requires large CPU times.

Note that the interpolation strategy can be advantageously used to predict the dynamic behavior of nearly periodic structures having spatially-varying mesh dispersion δ, i.e., which varies between the substructures (instead of being uniform). Switching from the uniform case to the non-uniform case does not require any new numerical task. This means: (i) computing eight reduced mass matrices $\widehat{\mathbf{M}}_p$ and eight reduced stiffness matrices $\widehat{\mathbf{K}}_p$ (see Eq. (29)) for a certain maximum dispersion $\delta_{\mathtt{max}}$; (ii) considering, for a given substructure s, random variables ϵ_x^s and ϵ_y^s with a "reduced" support $[-\delta^s\ ,\ \delta^s]$ (see Eq. (21)) where $\delta^s \leq \delta_{\mathtt{max}}$.

For instance, the dynamic response of a plate built from 4×4 randomly distorted substructures ($\delta^s = 0.01$) around the excitation point, and from undistorted substructures ($\delta^s = 0$) elsewhere else, can be predicted as shown in Fig. 13. In this case again, the vibrational energy remains confined around the excitation point. However, in this case, the energy appears to be strictly confined/bounded to the region occupied by the distorted substructures, while it is weak and uniformly spread everywhere else on the rest of the plate. This opens prospects towards the design of nearly periodic structures having such interesting features, e.g., which are able to "trap" the energy at some pre-determined positions.

4.4. Nearly periodic plate with 8×4 substructures embedded in a floor panel

A last example is considered which concerns a nearly periodic plate with 8×4 substructures, embedded in a floor panel (in steel) consisting in 96 homogeneous substructures (without distorted meshes). The whole

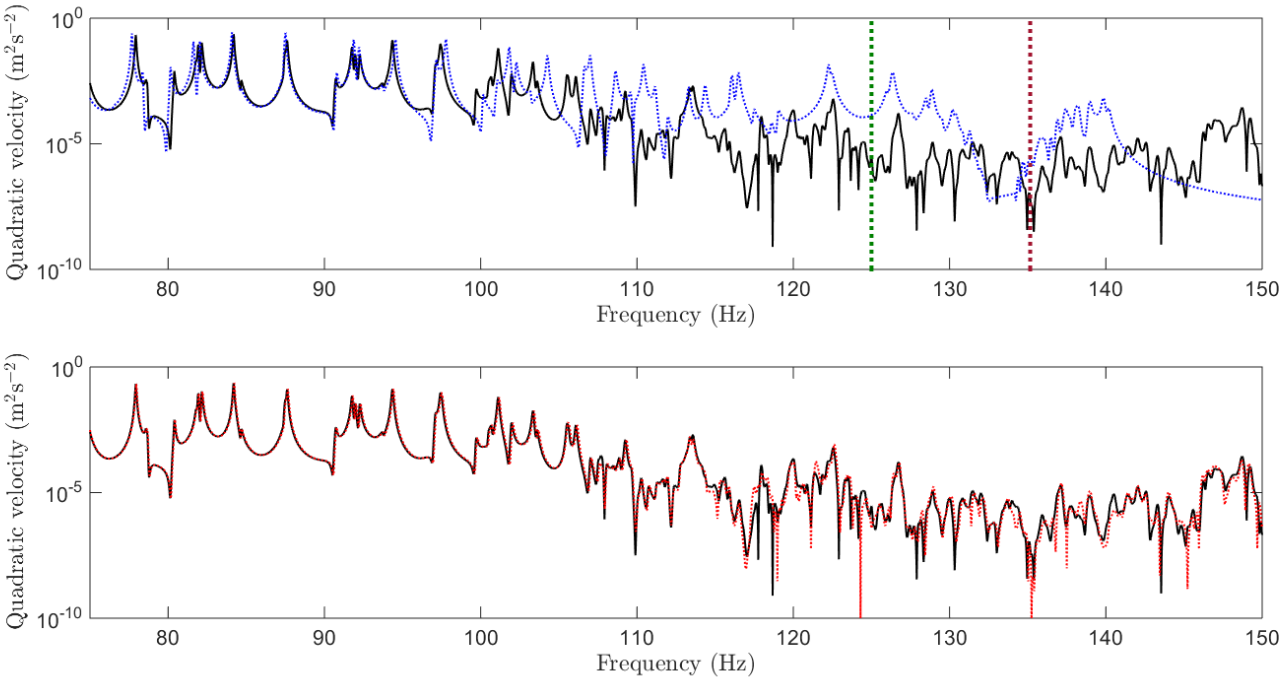

Figure 10: FRF (quadratic velocity) of the plate with 15×15 substructures. (black solid line) FE method, nearly periodic structure; (red dotted line) interpolation strategy, nearly periodic structure; (blue dotted line) FE method, purely periodic structure.

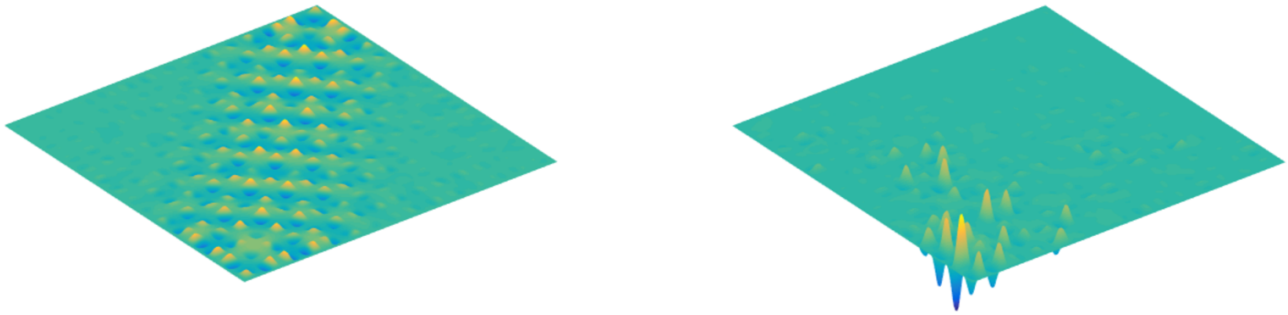

Figure 11: Transverse displacement field (real part) of the plate with 15×15 substructures at 125 Hz, obtained with the interpolation strategy. (left) Periodic case; (right) nearly periodic case.

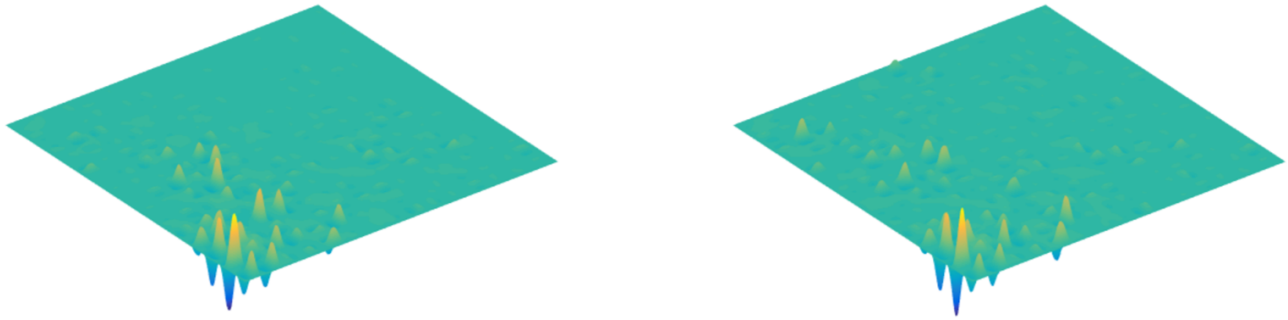

Figure 12: Transverse displacement field (real part) of the nearly periodic plate with 15×15 substructures at 125 Hz. (left) Interpolation strategy; (right) FE method.

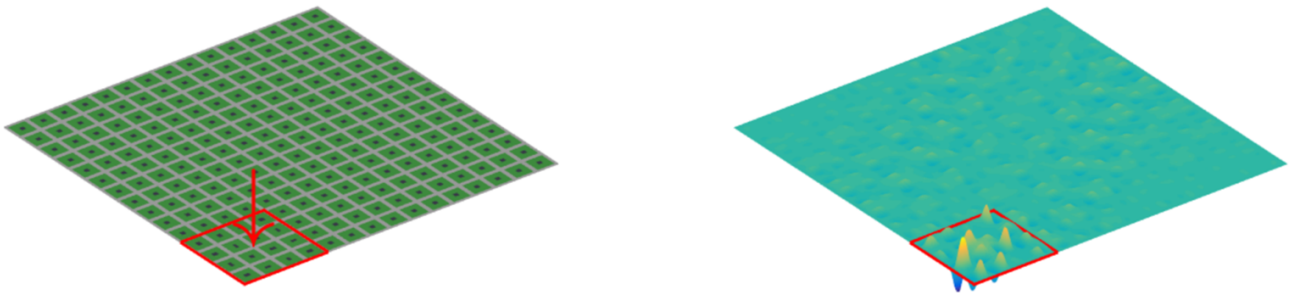

Figure 13: Periodic plate with 15×15 substructures including 4×4 randomly distorted substructures around the excitation point (red square region). (left) Schematic of the structure; (right) transverse displacement field at 125 Hz.

structure is simply supported along its edges, and it is subject to a vector of random point forces following a standard uniform distribution (between 0 and 1) which are applied at the corners of the substructures. A schematic of the structure is given in Fig. 14. Here, the mean value of the quadratic velocities measured at the locations of the excitation points is assessed. The related FRFs, for the nearly periodic and periodic plates with the floor panel, are plotted over $[0\,,\,150]$ Hz as shown in Fig. 15. The FRFs tend to differ for frequencies greater than 100 Hz in a similar way as in the previous cases. For instance, regarding the nearly periodic case at 125 Hz, the displacement field of the structure involves localized peaks of high magnitude in the plate, and small displacement levels in the floor (see Fig. 16). In comparison, the periodic case involves uniform (diffuse) field in the plate, and higher displacement levels in the floor. In this sense, the nearly periodic plate appears to be a suitable means to passively control the vibration levels of the floor.

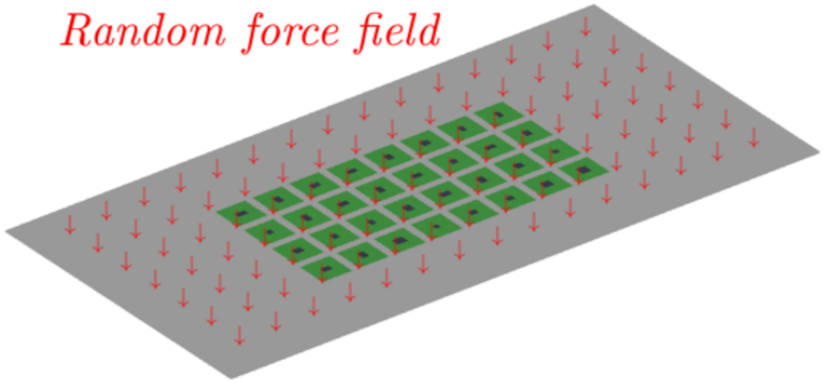

Figure 14: Schematic of a nearly periodic plate with 8×4 substructures with a floor panel subject to random forces.

Again, the interpolation strategy succeeds in describing the dynamic behavior of the structure, as shown in Figs. 15 and 17. The characteristics of the numerical models involved in the interpolation strategy and the FE method are given in Tab. 2. In this case, the interpolation strategy provides an overall time reduction of 86% compared to the FE method.

5. Conclusion

A numerical strategy based on matrix interpolation and distorted FE meshes has been proposed for modeling 2D nearly periodic structures. Such structures are made up of locally resonant substructures whose FE meshes differ and follow slight random variations in space. These substructures are usually modeled by means of reduced mass and stiffness matrices which are obtained through classic FE and CB procedures. For plane

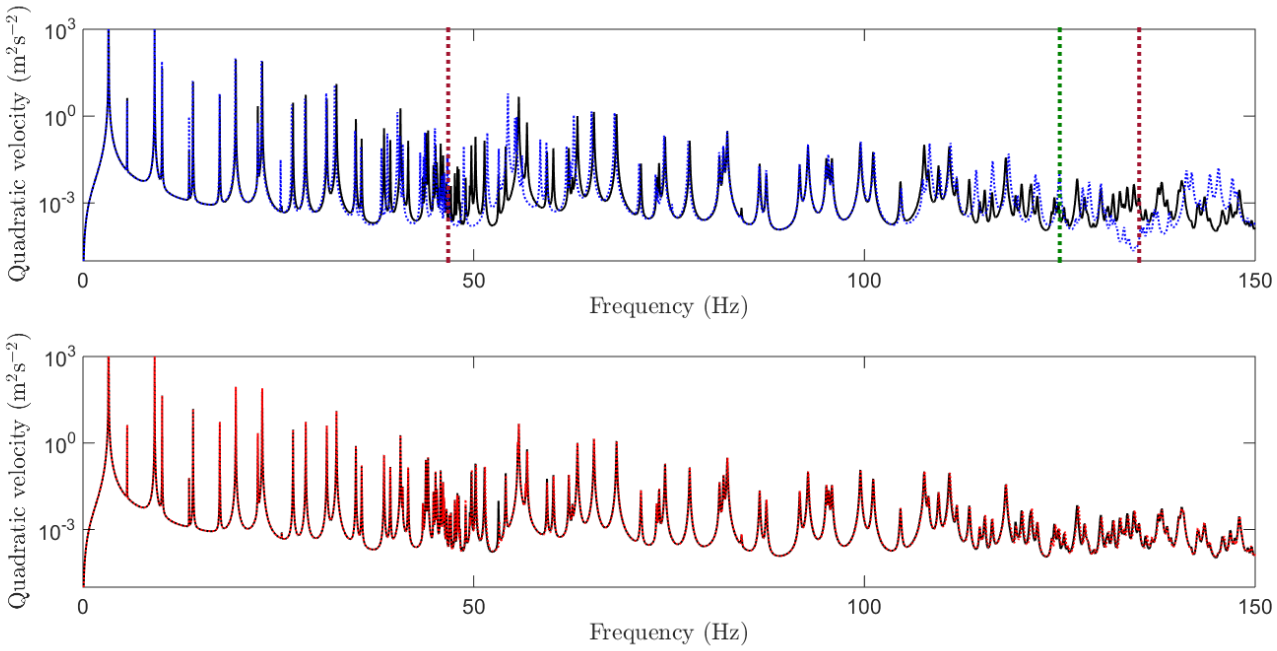

Figure 15: FRF (mean value of the quadratic velocity) of the plate with 8×4 substructures with the floor panel. (black solid line) FE method, nearly periodic structure; (red dotted line) interpolation strategy, nearly periodic structure; (blue dotted line) FE method, purely periodic structure.

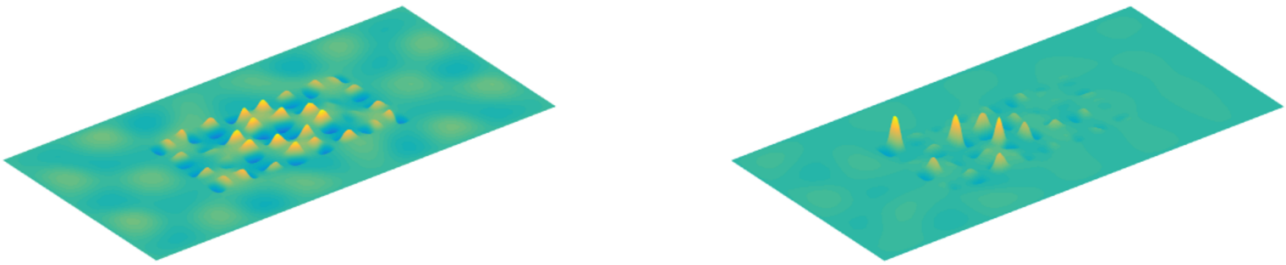

Figure 16: Transverse displacement field (real part) of the plate with 8×4 substructures with the floor panel at 125 Hz, obtained with the interpolation strategy. (left) Periodic case; (right) nearly periodic case.

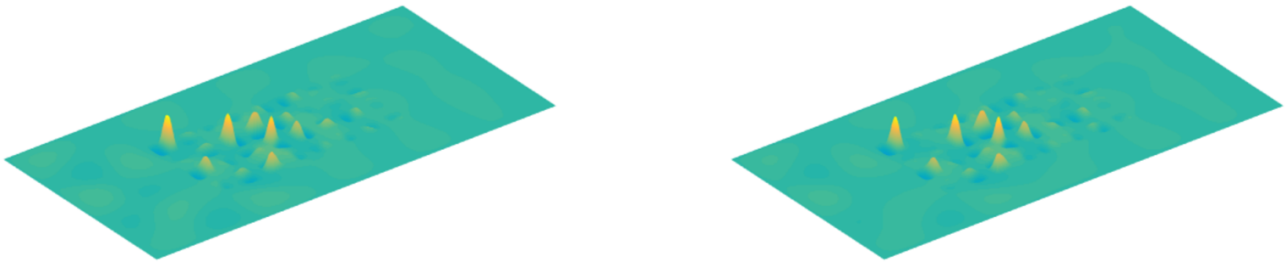

Figure 17: Transverse displacement field (real part) of the nearly periodic plate with 8×4 substructures with the floor panel at 125 Hz. (left) Interpolation strategy; (right) FE method.

substructures, random variations of their geometrical parameters have been considered by perturbing the node coordinates (x_j^e, y_j^e), for a given substructure s, as $x_j^e + \epsilon_x^s f_x(x_j^e, y_j^e)$ and $y_j^e + \epsilon_y^s f_y(x_j^e, y_j^e)$ where $f_x(x_j^e, y_j^e)$ and $f_y(x_j^e, y_j^e)$ are two deterministic functions, and ϵ_x^s and ϵ_y^s are two random variables. Since the substructures are different, their reduced mass and stiffness matrices have to be computed as many times as the number

of substructures considered, which can be highly cumbersome. The proposed strategy aims at solving this issue. It involves computing the reduced mass and stiffness matrices of the substructures for some coordinates $\epsilon_x^s = (\epsilon_x)_p$ and $\epsilon_y^s = (\epsilon_y)_p$ whose number is small, and interpolating the reduced matrices elsewhere between these "interpolation points". The proposed strategy has been used to analyze the harmonic behavior of three structures with resonant layered substructures, i.e., a plate with 8×8 substructures, a plate with 15×15 substructures, and a plate with 8×4 substructures embedded in a floor panel. The relevance of the interpolation strategy, in terms of computational load saving and accuracy, has been highlighted through comparisons with the FE method (with a model reduction based on the global modes of the structures) and the CB method. It has been shown that the proposed strategy is roughly $80 - 90\%$ faster than the FE method, while the CB method requires a high computational load. The analysis of these three structures has revealed two interesting features about nearly periodic structures, i.e., (i) the vibrational energy is localized around the excitation sources, and (ii) overall the vibration levels are small compared to the purely periodic cases. Follow-on works could include the analysis of 2D nearly periodic structures made up of 3D substructures with more complex topologies.

References

[1] M. Castanier, C. Pierre, Individual and interactive mechanisms for localization and dissipation in a mono-coupled nearly-periodic structure, Journal of Sound and Vibration 168 (3) (1993) 479–505.

[2] F.-M. Li, Y.-S. Wang, Study on wave localization in disordered periodic layered piezoelectric composite structures, International Journal of Solids and Structures 42 (2005) 6457–6474.

[3] M. Hussein, Reduced Bloch mode expansion for periodic media band structure calculations, Proceedings of the Royal Society A 465 (2009) 2825–2848.

[4] D. Krattiger, M. Hussein, Generalized Bloch mode synthesis for accelerated calculation of elastic band structures, Journal of Computational Physics 357 (2018) 183–205.

[5] A. Palermo, A. Marzani, Extended Bloch mode synthesis: Ultrafast method for the computation of complex band structures in phononic media, International Journal of Solids and Structures 100–101 (2016) 29–40.

[6] M. Collet, M. Ouisse, M. Ruzzene, M. Ichchou, Floquet-Bloch decomposition for the computation of dispersion oftwo-dimensional periodic, damped mechanical systems, International Journal of Solids and Structures 48 (20) (2011) 2837–2848.

[7] A. Phani, J. Woodhouse, N. Fleck, Wave propagation in two-dimensional periodic lattices, The Journal of the Acoustical Society of America 119 (4) (2006) 1995–2005.

[8] A.-L. Chen, Y.-S. Y.-S. Wang, Study on band gaps of elastic waves propagating in one-dimensional disordered phononic crystals, Physica B: Condensed Matter 392 (2007) 369–378.

[9] M. Hussein, G. Hulbert, R. Scott, Dispersive elastodynamics of 1D banded materials and structures: Design, Journal of Sound and Vibration 307 (2007) 865–893.

[10] R. R. Craig, M. C. C. Bampton, Coupling of substructures for dynamic analyses, AIAA Journal 6 (7) (1968) 1313–1319.

[11] M. Géradin, D. Rixen, Mechanical Vibrations: Theory and Application to Structural Dynamics, Wiley, Paris, 1994.

[12] R. Langley, The response of two-dimensional periodic structures to point harmonic forcing, Journal of Sound and Vibration 197 (4) (1996) 447–469.

[13] D. Duhamel, Finite element computation of Green's functions, Engineering Analysis with Boundary Elements 31 (11) (2007) 919–930.

[14] S. Balmès, Parametric families of reduced finite element models theory and applications, Mechanical Systems and Signal Processing 10 (4) (1996) 381–394.

[15] S. Balmès, Optimal Ritz vectors for component mode synthesis using the singular value decomposition, AIAA Journal 34 (1996) 1256–1260.

[16] G. Masson, B. A. Brik, S. Cogan, N. Bouhaddi, Component mode synthesis (CMS) based on an enriched ritz approach for efficient structural optimization, Journal of Sound and Vibration 296 (2006) 845–860.

[17] S.-K. Hong, B. Epureanu, M. Castanier, Next-generation parametric reduced-order models, Mechanical Systems and Signal Processing 37 (2013) 403–421.

[18] H. Panzer, J. Mohring, R. Eid, B. Lohmann, Parametric model order reduction by matrix interpolation, at-Automatisierungstechnik 58 (8) (2010) 475–484.

[19] D. Amsallem, C. Farhat, An Online Method for Interpolating Linear Parametric Reduced-Order Models, SIAM Journal on Scientific Computing 33 (5) (2011) 2169–2198.

[20] B. Goller, H. Pradlwarter, G. Schuëller, An interpolation scheme for the approximation of dynamical systems, Computer Methods in Applied Mechanics and Engineering 200 (2011) 414–423.

[21] J. Lee, M. Cho, An interpolation-based parametric reduced order model combined with component mode synthesis, Computer Methods in Applied Mechanics and Engineering 319 (2017) 258–286.

[22] P. Papadopoulos, Introduction to the finite element method, University of California, Berkeley, 2010.

[23] O. Zienkiewicz, R. Taylor, J. Zhu, The Finite Element Method: Its Basis and Fundamentals, Elsevier Butterworth-Heinemann, sixth edition, Oxford, 2005.

[24] E. Hinton, B. Bicanic, A comparison of Lagrangian and Serendipity Mindlin plate elements for free vibration analysis, Computers and Structures 10 (1979) 483–493.

[25] K.-J. Bathe, E. Dvorkin, A four-node plate bending element based on Mindlin/Reissner theory and a mixed interpolation, International Journal for Numerical Methods in Engineering 21 (1985) 367–383.

[26] T. Davis, Creating sparse Finite-Element matrices in MATLAB, http://blogs.mathworks.com/loren/2007/03/01/creating-sparse-finite-element-matrices-in-matlab/.

Appendix. Mass and stiffness matrices of isoparametric Mindlin plate elements

An eight-node isoparametric Mindlin plate element is defined by means of three DOFs per node, i.e., the transverse displacement w along axis z and the section rotations θ_x and θ_y about axes x and y. The related mass and stiffness matrices (size 24×24) are expressed by:

$$\mathbf{M}^e = \rho^e h^e \int_{\xi=-1}^{1} \int_{\eta=-1}^{1} (\mathbf{N}^e)^T \mathbf{I}^e \mathbf{N}^e \, J^e \, d\xi d\eta, \tag{A-1}$$

and

$$\mathbf{K}^e = h^e \int_{\xi=-1}^{1} \int_{\eta=-1}^{1} (\mathbf{B}_{\mathtt{f}}^e)^T \mathbf{H}_{\mathtt{f}}^e \mathbf{B}_{\mathtt{f}}^e \, J^e \, d\xi d\eta + h^e \int_{\xi=-1}^{1} \int_{\eta=-1}^{1} (\mathbf{B}_{\mathtt{s}}^e)^T \mathbf{H}_{\mathtt{s}}^e \mathbf{B}_{\mathtt{s}}^e \, J^e \, d\xi d\eta, \tag{A-2}$$

where the dependency of matrices and scalars on the parametric coordinates (ξ, η) is not highlighted for the sake of conciseness. The matrix $\mathbf{N}^e$ occurring in Eq. (A-1) is given by:

$$\mathbf{N}^e = \left[\begin{array}{ccc|ccc|c|c} N_1^e & 0 & 0 & N_2^e & 0 & 0 & \cdots & 0 \\ 0 & N_1^e & 0 & 0 & N_2^e & 0 & \cdots & 0 \\ 0 & 0 & N_1^e & 0 & 0 & N_2^e & \cdots & N_8^e \end{array}\right], \tag{A-3}$$

where N_j^e $(j = 1, \ldots, 8)$ are the interpolation functions which are of serendipity type, see Eq. (32). Also, the matrix $\mathbf{I}^e$ is defined as follows:

$$\mathbf{I}^e = \begin{bmatrix} 1 & 0 & 0 \\ 0 & \frac{(h^e)^2}{12} & 0 \\ 0 & 0 & \frac{(h^e)^2}{12} \end{bmatrix}. \tag{A-4}$$

The matrices $\mathbf{B}_{\mathtt{f}}^e$ and $\mathbf{B}_{\mathtt{s}}^e$ occurring in Eq. (A-2) are given by:

$$\mathbf{B}_{\mathtt{f}}^e = \left[\begin{array}{ccc|ccc|c|c} 0 & 0 & \frac{\partial N_1^e}{\partial x} & 0 & 0 & \frac{\partial N_2^e}{\partial x} & \cdots & \frac{\partial N_8^e}{\partial x} \\ 0 & -\frac{\partial N_1^e}{\partial y} & 0 & 0 & -\frac{\partial N_2^e}{\partial y} & 0 & \cdots & 0 \\ 0 & -\frac{\partial N_1^e}{\partial x} & \frac{\partial N_1^e}{\partial y} & 0 & -\frac{\partial N_2^e}{\partial x} & \frac{\partial N_2^e}{\partial y} & \cdots & \frac{\partial N_8^e}{\partial y} \end{array}\right], \tag{A-5}$$

and

$$\mathbf{B}_{\mathtt{s}}^e = \left[\begin{array}{ccc|ccc|c|c} \frac{\partial N_1^e}{\partial x} & 0 & N_1^e & \frac{\partial N_2^e}{\partial x} & 0 & N_2^e & \cdots & N_8^e \\ \frac{\partial N_1^e}{\partial y} & -N_1^e & 0 & \frac{\partial N_2^e}{\partial y} & -N_2^e & 0 & \cdots & 0 \end{array}\right]. \tag{A-6}$$

Finally, the matrices $\mathbf{H}_{\mathtt{f}}^e$ and $\mathbf{H}_{\mathtt{s}}^e$ are given by:

$$\mathbf{H}_{\mathtt{f}}^e = \frac{E^e (h^e)^2}{12\,(1 - (\nu^e)^2)} \begin{bmatrix} 1 & \nu^e & 0 \\ \nu^e & 1 & 0 \\ 0 & 0 & \frac{1-\nu^e}{2} \end{bmatrix}, \tag{A-7}$$

and

$$\mathbf{H}_{\mathtt{s}}^e = \frac{E^e \kappa}{2(1+\nu^e)} \begin{bmatrix} 1 & 0 \\ 0 & 1 \end{bmatrix}, \tag{A-8}$$

where E^e is the Young's modulus, ν^e is the Poisson's ratio, and $\kappa = 5/6$ is the shear correction factor.

- Dynamic analysis of 2D nearly periodic structures made up of different substructures whose geometrical properties randomly vary in space.
- Application to 2D resonant metamaterials made up of layered substructures.
- Use of distorted FE meshes for modeling the substructures.
- Model reduction based on the interpolation of the reduced (mass and stiffness) matrices of the substructures.
- Numerical experiments involving nearly periodic plates (Mindlin) made up of locally resonant substructures.

Declaration of interests

☒ The authors declare that they have no known competing financial interests or personal relationships that could have appeared to influence the work reported in this paper.

☐The authors declare the following financial interests/personal relationships which may be considered as potential competing interests:
